Fall 12-15-2016

Analysis of traveling wave propagation in one-dimensional integrate-and-fire neural networks

Jie Zhang
Georgia State University

TITLE: ANALYSIS OF TRAVELING WAVE PROPAGATION IN ONE-DIMENSIONAL INTEGRATE-AND-FIRE NEURAL NETWORKS

by

JIE ZHANG

Under the Direction of Remus Mihai Osan, PhD

ABSTRACT

One-dimensional neural networks comprised of large numbers of Integrate-and-Fire neurons have been widely used to model electrical activity propagation in neural slices. Despite these efforts, the vast majority of these computational models have no analytical solutions. Consequently, my Ph.D. research focuses on a specific class of homogeneous Integrate-and-Fire neural network, for which analytical solutions of network dynamics can be derived. One crucial analytical finding is that the traveling wave acceleration quadratically depends on

the instantaneous speed of the activity propagation, which means that two speed solutions exist in the activities of wave propagation: one is fast-stable and the other is slow-unstable.

Furthermore, via this property, we analytically compute temporal-spatial spiking dynamics to help gain insights into the stability mechanisms of traveling wave propagation. Indeed, the analytical solutions are in perfect agreement with the numerical solutions. This analytical method also can be applied to determine the effects induced by a non-conductive gap of brain tissue and extended to more general synaptic connectivity functions, by converting the evolution equations for network dynamics into a low-dimensional system of ordinary differential equations.

Building upon these results, we investigate how periodic inhomogeneities affect the dynamics of activity propagation. In particular, two types of periodic inhomogeneities are studied: alternating regions of additional fixed excitation and inhibition, and cosine form inhomogeneity. Of special interest are the conditions leading to propagation failure. With similar analytical procedures, explicit expressions for critical speeds of activity propagation are obtained under the influence of additional inhibition and excitation. However, an explicit formula for speed modulations is difficult to determine in the case of cosine form inhomogeneity. Instead of exact solutions from the system of equations, a series of speed approximations are constructed, rendering a higher accuracy with a higher order approximation of speed.

INDEX WORDS: Traveling waves, Integrate-and-fire neuron model, Propagation failure, Differential equations, Speed approximations, Numerical simulations

TITLE: ANALYSIS OF TRAVELING WAVE PROPAGATION IN INTEGRATE-AND-FIRE NEURAL NETWORKS

by

JIE ZHANG

A Dissertation Submitted in Partial Fulfillment of the Requirements for the Degree of

Doctor of Philosophy

in the College of Arts and Sciences

Georgia State University

2016

TITLE: ANALYSIS OF TRAVELING WAVE PROPAGATION IN ONE-DIMENSIONAL INTEGRATE-AND-FIRE NEURAL NETWORKS

by

JIE ZHANG

Committee Chair: Remus Mihai Osan

Committee: Gennady Cymbalyuk

Igor Belykh

Yi Jiang

Electronic Version Approved:

Office of Graduate Studies

College of Arts and Sciences

Georgia State University

December 2016

DEDICATION

This dissertation is dedicated to my parents, Zhengfu Zhang and Junfei Gao, who have always loved me unconditionally and whose good examples have taught me to work hard for the things that I aspire to achieve.

ACKNOWLEDGEMENTS

First and foremost, I would like to express my deepest gratitude to my Ph.D. advisor, Dr. Remus Osan, for his consistent support, guidance, and inspiration for the past five years. Besides of a broad spectrum of quantitative skills and methods that I've learned from Dr. Remus Osan, the most valuable skill, I think, is critical thinking that enables me to face and solve novel and challenging problems in the future. I feel so fortunate to have the chance to work with him.

Moreover, I am grateful that I was enrolled in the Department of Mathematics & Statistics at Georgia State University. Thanks go to our Chair and Directors, Dr. Guantao Chen, Dr. Gengsheng Qin, Dr. Zhongshan Li, Dr. Florian Enescu for providing academic advice and help. Also, I want to express my sincere gratitude to Professor Vladimir Bondarenko, Alexandra Smirnova, Michael Steward for serving on my qualifying exam committee and Professor Gennady Cymbalyuk, Igor Belykh, Jiang Yi for serving on my Ph.D. dissertation committee.

In addition, I would like to acknowledge my family for always encouraging me to do research and all my friends who have offered their support and assistance in this journey. Again, thanks to Dr. Osan, who is always there being patient and supportive in my five-year Ph.D. program and help me grow and develop to be professional in Bioinformatics. Without him, I would not be able to go this far.

Support

My Ph.D. research was partially supported by a Georgia State Brain and Behavior Fellowship in 2015, a Research Initiation Grant at Georgia State University, a Brain and Behavior Seed Grant at Georgia State University to Dr. Remus Osan.

TABLE OF CONTENTS

LIST OF TABLES

LIST OF FIGURES

LIST OF ABBREVIATIONS

- GSU - Georgia State University
- ODE - Ordinary Differential Equation
- PDE - Partial Differential Equation
- HH model - Hodgkin-Huxley model
- LIF - Leaking Integrate-and-Fire model
- EIF - Exponential Integrate-and-Fire model
- SNIC - Saddle-Node on a Limit Cycle Bifurcation
- QIF - Quadratic Integrate-and-Fire model
- HR model - Hindmarsh and Rose Model
- FLOPS - Approximate Number of Floating Point Operations
- V1 - Human Primary Visual Cortex
- GABA - Gamma-Aminobutyric Acid (γ-Aminobutyric acid)
- NDF - Numerical Differentiation Formula
- BDF - Backward Differentiation Formula

CHAPTER 1

INTRODUCTION

1.1 Motivations

The human brain has about 100 billion neurons, and each of them may be connected to up to 10,000 other neurons, passing signals to each other via as many as 1,000 trillion synaptic connections. Not surprisingly, the dynamics of electrical neural activity are complicated and challenging to quantify and interpret. Many scientists and researchers have devoted to this area, including the research in the visual [1–6], olfactory [7, 8], auditory [9, 10], somatosensory [11] and motor cortices [12]. Traveling waves of electrical activity are formed by neurons interactions that pass signals through the whole network. Research has shown that traveling waves are playing important roles in sensory processing [13], phase coding [14] and sleep [15]. Also, the existence of traveling waves for hippocampal theta oscillations has been found [16, 17], which may act as local clocks to govern spatial-temporal dynamics.

Traveling waves are natural dynamics that are ubiquitous to neural networks. Therefore, this area of research is essential not only for understanding the functions of the brain during sensory processing but also for providing insights into irregular neural dynamics [18] or abnormal states such as epileptic seizure [19,20], migraine [21], hallucination [22,23] and the ones observed after brain injury [24]. This highlights the need for further research in this area that uses both analytical and computational methods.

Computational models are widely used to understand the dynamics of traveling waves in neural tissue, yet due to model's complexity, analytical solutions are scarce. These models usually describe the neural tissue as a vast interconnected network of homogeneous excitatory units, such as firing rate models [25–28], integrate and fire models [25, 29–34], theta neuron models [35, 36] or more complex models of neurons [29, 37–44]. In these models, traveling wave propagation has been studied numerically in an extensive fashion using the assumptions

that the strength of the synaptic connections between neurons depends only on the distance between them and that this interaction does not depend on other local parameters.

The assumptions listed above make it possible to formulate a set of integro-differential equations describing the propagation of the one-spike traveling wave fronts in a continuous one-dimensional Integrate-and-Fire neural network. Typically, these models give rise to a pair of traveling wave speed solutions, where the slower wave is unstable, and the fast one is stable.

Using these equations, the transition between initiation and evolution toward constant speed traveling waves for Gaussian connectivity [31] and finite support connectivity [33] has been studied and results were derived analytically. The analytical results were further confirmed by numerical simulations, leading to methods for optimizing and improving simulations of large-scale networks [34]. These results also apply to the case of constant speed waves with a finite and an infinite number of spikes [32] .

This framework has produced insights into the mechanisms of stable constant-speed traveling wave solutions in homogeneous media, but there are additional microstructures that could modify the dynamics of traveling wave propagation. Among those, some have an approximately periodic structure, for example in the primary visual cortex and the cerebral cortex [45,46]. These periodic structures motivate us to continue the work on the propagation activities of traveling waves under the influence of periodic inhomogeneity modulation that act in addition to the homogeneous interaction described above.

So far the study of inhomogeneity in synaptic connections likely to exist in the brain tissue has received much less attention since, not surprisingly, the presence of inhomogeneity vastly increases the complexity of the mathematical models. Among the existing studies of wave propagations in an inhomogeneous neural network, spatial averaging and homogenization theory have been used to determine an analytical expression of average wave speed and the transition between propagation success and its failure [45, 47, 48]. This was derived under the assumption that the perturbation is sufficiently small such that the periodic modulation occurs on a smaller length scale than the correlation length of the coupling function

in various continuous and discrete models.

Based on the work by Ermentrout and Osan [31–34], an evolution expression of traveling wave firing activities is obtained. In a collaboration with Osan, I have derived exact speed solutions in a homogeneous neural network, which was published in an recent paper [49].

Furthermore, we explore the dynamics under the influence of periodic inhomogeneity and believe that the methods we have used to find analytical solutions of wave speed accurately capture the transition between propagation success and failure. In turn, this provides us additional and valuable information about the dynamics of propagation activities and propagation failure conditions.

These methods could also be extended to multi-spiking neural networks, neural networks with non-conductive gaps and networks with more general synaptic connectivity functions.

1.2 Biological neuron models

Spiking neurons are known to be the major signaling unit of the nervous system, though not all the cells are spiking neurons. For example, the cochlear hair cells, retinal receptor cells, and retinal bipolar cells do not generate spikes. Furthermore, many cells are classified as glia instead of neurons [50]. To characterize spiking neurons activities, several spiking neuron models have been developed by researchers. Basically, they are mathematical models of the electrical properties of neuronal action potentials, which have abrupt changes in the voltage across the cell membrane.

There are mainly two categories for neuron models according to the input form: electrical input/output membrane voltage models and natural input neuron models. Electrical input/output membrane voltage models have output voltage as a function of electrical input. These models are different in the exact functional relationship between their input current and the output. Some models even do not have an implicit functional relationship, and we can only tell through two measured voltage levels: the presence of a spike or a quiescent state. Natural input neuron models involve natural stimulation as mostly used in experiments. The results from these experiments tend to change from trial to trial, but the averaged response

tends to converge to a clear pattern. Accordingly, the output of natural neuron models is the probability of a spike event as a function of the input stimulus. Typically, the output probability is normalized or divided by a time constant, and the resulting normalized probability is called the "firing rate" with units of Hertz. The models in this category differ in the functional relationship connecting the input current to the output probability. Markov models are the simplest and yield the most tractable results in the category of natural input neuron models [50].

The models with electrical input and output membrane voltage describe the relationship between neuronal input currents and the output voltage. In the early 1950s, Hodgkin and Huxley made the most extensive experimental inquiry in this category of models using an experimental setup that punctured the cell membrane and allowed to force a specific membrane voltage or current. Currently, extracellular electrical stimulation is also used in the experimental electrical neural input to avoid membrane puncturing which can lead to cell death and tissue damage.

1.2.1 Integrate-and-Fire Model

In the study of network dynamics, computational models are widely used to simulate the neuron network dynamics. Izhikevich has discussed the biological plausibility from the perspective of how many neuron/network features can be modeled and the computational efficiency of some of the most useful models of spiking and bursting neurons[51]. Among them, Integrate-and-Fire model is the simplest model to implement as one of the most suitable models to prove analytical results.

Over years, scientists and researchers have explored and discovered more details of the structure and function of the brain. As the primary processing units in the central nervous system, neurons are wired in a way that optimizes the interactions with each other in various forms in the brain. Typically, a neuron has three parts: dendrites, soma, and axon.

Dendrites receive signals from other neurons and transmit them to the cell body, or soma, where signals are processed in a non-linear form: if the total input signal reaches a

certain threshold (denoted by η), then an output signal (also called action potential) will be generated. In the event that the membrane potential reaches the threshold, it is said that the neuron fires or spikes. In 1907, Louis Lapicque first investigated the neuron model [52], which is the derivative of the law of capacitance, $Q = CV$, with respect to time,

$$I(t) = C_m \frac{dV_m(t)}{dt}. \tag{1.1}$$

When an input current is applied, the membrane voltage increases with time until it reaches a certain threshold V_{th}. At this point the neuron elicits a pulse and the voltage is reset to its resting potential, after which the neuron continues integrating voltage. In this original model, the firing frequency of the neuron is linearly increasing with the increase of input current without an upper bound.

To fix this shortcoming, a refractory period t_{ref} was introduced so that the firing frequency of a neuron is limited [53]. Through some calculations that involve the Fourier transformation, one can show that firing frequency is a function of constant input current, which takes the following form:

$$f(I) = \frac{I}{C_m V_{th} + t_{ref} I}. \tag{1.2}$$

One of the shortcomings of this model is that it does not have time-dependent memory, which means that when the model receives a signal at some time below the threshold, it will retain that voltage forever until it reaches the threshold and fires action potential.

In the leaky integrate-and-fire model (LIF model), a "*leak*" term is added to the membrane potential. This simulates the diffusion of ions, which occurs through the membrane when the threshold is not reached in the cell. This leaking term solves the memory problem, and the model looks as follows,

$$I(t) - \frac{V_m(t)}{R_m} = C_m \frac{dV_m(t)}{dt}, \tag{1.3}$$

where R_m is the membrane resistance. The voltage threshold is

$$I_{th} = V_{th}/R_m. \tag{1.4}$$

The neuron fires once the voltage exceeds the threshold. Otherwise, it will simply leak out the excessed ions until the potential reaches the resting voltage. The firing frequency has the following expression:

$$f(I) = \begin{cases} 0, & I \leq I_{th}, \\ [t_{ref} - R_m C_m log(1 - \frac{V_{tm}}{IR_m})]^{-1}, & I > I_{th}, \end{cases}$$

when the input current is getting large, it converges to the previous leak-free model with refractory period.

Also, by the form of spiking generation, the Exponential Integrate-and-Fire (EIF) model was proposed [54] that the neurons spike in the form of exponential function, following the equation:

$$\frac{dX}{dt} = \Delta_T exp(\frac{X - X_T}{\Delta_T}), \tag{1.5}$$

where X is the membrane potential, X_T is the membrane potential threshold, and Δ_T is the rate of action potential initiation, usually around $1mV$ for cortical pyramidal neurons. Once the membrane potential crosses the threshold (X_T), it diverges to infinity in finite time.

Figure 1.1 illustrates the subthreshold dynamics of the Integrate-and-Fire model without additional injections and spiking activities with extra injecting current($1nA$) from $100ms$ to $400ms$, where the spiking threshold is $-55mV$, the resting potential is $-70mV$ and the reset potential is $-75mV$. Below the threshold(Fig.1.1(a)), the Integrate-and-Fire neuron acts as a leaky capacitor whose voltage, in the absence of injected current, decays to the resting potential. But with injected current(Fig.1.1(b)) that drives the voltage reaching the spiking threshold, the voltage jumps to a higher level and it is immediately reset to a hyperpolarized

level $V = -75mV$.

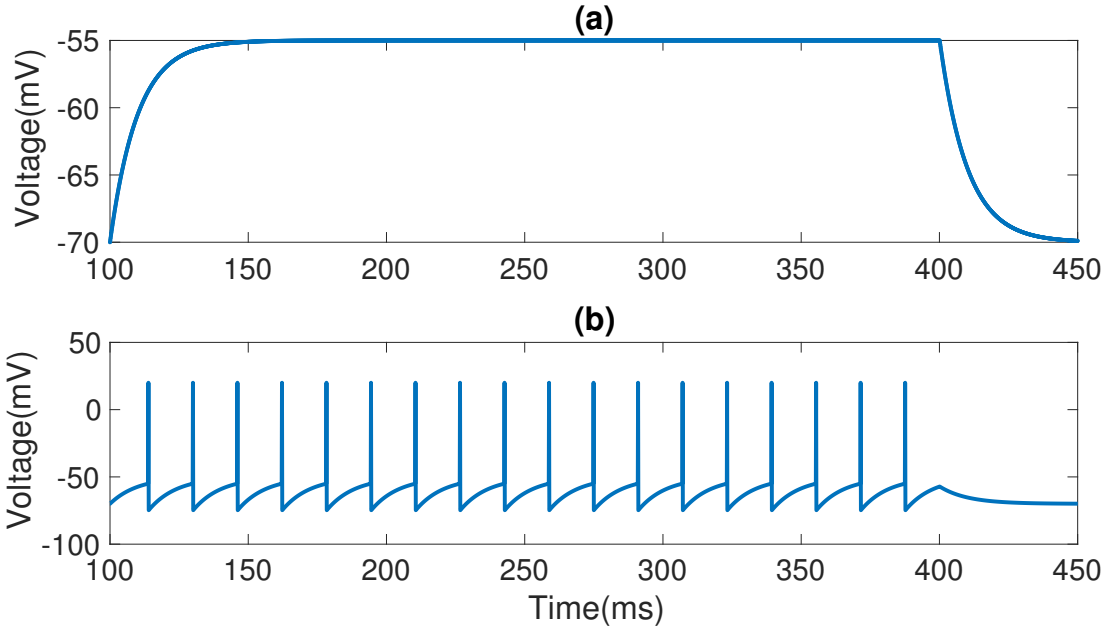

Figure (1.1) **Dynamcis of Integrate-and-Fire neuron model.** (a) **Subthreshold voltage dynamics.** Below threshold, the neuron integrates voltage and exponentially decays to resting potential. (b) **Spiking dynamics.** Due to injected currents($I = 1nA$), the voltage reaches the action potential threshold $V_T = -55mV$ and the neuron spikes immediately to a higher level($V = 20mV$). Then it is immediately reset to a hyperpolarized level $-75mV$.

A specific instance of a nonlinear integrate-and-fire model is the Quadratic Integrate-and-Fire Model (QIF) created by Latham et al. in 2000 to model the network of spiking neurons with low firing rate [55],

$$\tau \frac{du}{dt} = a_0(u - u_{rest})(u - u_c) + RI, \tag{1.6}$$

with parameters $a_0 > 0$ and $u_c > u_{rest}$. For $I = 0$ and initial condition $u < u_c$, the voltage decays to the resting potential u_{rest}. For $u > u_c$ it increases so that an action potential is triggered. $u_c$can be interpreted as the critical voltage for spiking initiation.

Similar models include the theta model, which is a related model that can be obtained from the QIF model through a nonlinear change of the coordinates.

1.2.2 Ermentrout-Kopell Canonical Model

The Ermentrout-Kopell canonical model, also called the "Θ neuron", was first brought up by Ermentrout and Kopell in 1986 [56]. It is a simple one-dimensional phase model for spiking neurons with only one state variable (θ) which is a variable changed from the membrane voltage of a neuron. The model takes the following differential equation:

$$\frac{d\theta}{dt} = 1 - cos(\theta) + (1 + cos(\theta))I(t). \tag{1.7}$$

where $I(t)$ is the input to the model. The variable θ lies on the unit circle and ranges between 0 and 2π. When $\theta = \pi$ the neuron spikes, that is, it produces an action potential.

The advantage of the Θ-Neuron over the QIF model is that there is no reset to deal with and, as a consequence of removing this discontinuity, the resulting dynamics are smooth and stay bounded. This model also allows for explicit expressions for the dynamics of spiking neurons activities. Particularly, theta model is well formed to describe neuron bursting, which is often found in neurons responsible for controlling and maintaining steady rhythms [57]. Osan et al. (2002) [35] have found that in a network of theta neurons, there exist two different types of waves that propagate smoothly over the network, given a sufficiently large coupling strength.

1.2.3 Hodgkin-Huxley Model and its Extensions

The Hodgkin-Huxley model (HH model) [58–61] factors in the ion currents crossing the neuronal cell membrane and the membrane voltage explicitly. Basically, Hodgkin-Huxley model includes voltage-gated ion channels and leak channels. Leak channels account for the natural permeability of the membrane to ions and have the same mathematical form as the voltage-gated channels. The voltage-gated channels are characterized by the channel

conductance g_i which is a function of both time and voltage.

The model is based on experiments that allowed forcing membrane voltage using an intracellular pipette on the axons of giant squid neurons. In 1963, Hodgkin and Huxley won the Nobel Prize for their work in Physiology.

HH model was generalized to include multiple voltage-dependent currents as stated above. Here are the equations for the voltage-current relationship:

$$C_m \frac{dV(t)}{dt} = -\sum_i I_i(t, V). \tag{1.8}$$

Each current is given by Ohm's Law as

$$I(t, V) = g(t, V) \cdot (V - V_{eq}), \tag{1.9}$$

where $g(t, V)$ is the conductance, or inverse resistance, which can be expanded in terms of its constant average $\bar{g}$ and the activation and inactivation fractions m and h. m and h are dimensionless gate variables. The conductance determines how many ions can flow through available membrane channels. This expansion is given by

$$g(t, V) = \bar{g} \cdot m(t, V)^p \cdot h(t, V)^q, \tag{1.10}$$

and m, h are the gate variables defined by the first-order differential equations, such as,

$$\frac{dm(t, V)}{dt} = \frac{m_\infty(V) - m(t, V)}{\tau_m(V)} = \alpha_m(V) \cdot (1 - m) - \beta_m(V) \cdot m, \tag{1.11}$$

with similar dynamics for h, where we can use either τ and m_{inf} or α and β to define the gate variables.

This formulation allows considerable flexibility in the inclusion of ion currents. Typically, these terms include inward Ca^{2+} and Na^+ input currents and several varieties of K^+

outward currents, including a "leak" current.

From the expressions of Hodgkin-Huxley model, there are gate variables for each ion channel and each gate variable has two parameters that need to estimate. Also, the channel conductance ($g(V, x)$) is important to measure for the model simulation. For complex systems of neurons, it is not easily tractable by computer. Careful simplifications of the Hodgkin-Huxley model are therefore needed.

Great simplifications to the Hodgkin-Huxley model were introduced by FitzHugh and Nagumo in 1961 and 1962 [62]. It is a model that incorporates non-linear positive-feedback membrane voltage and a linear negative-feedback recovery variable (ω). The model is described in the following expressions,

$$\frac{dV}{dt} = V - V^3 - \omega + I_{ext}, \tag{1.12}$$

$$\tau\frac{d\omega}{dt} = V - a - b\omega, \tag{1.13}$$

where the model has a membrane voltage and input current with a slower general gate variable ω and experimentally-determined parameters $a = -0.7, b = 0.8, \tau = 1/0.08$. Although not clearly derivable from biology as HH model, FitzHugn-Nagumo model allows for simplified, immediately available dynamics of spiking neurons.

In 1981, Morris and Lecar [63] combined Hodgkin-Huxley model and FitzHugh Nagumo model into a voltage-gated calcium channel model with a delayed-rectifier potassium channel, represented by

$$C\frac{dV}{dt} = -I_{ion}(V, \omega) + I, \tag{1.14}$$

$$\frac{d\omega}{dt} = \phi \cdot \frac{\omega_\infty - \omega}{\tau_\omega}, \tag{1.15}$$

wehre $I_{ion}(V, \omega) = \bar{g}_{Ca} m_\infty \cdot (V - V_{Ca}) + \bar{g}_K \omega \cdot (V - V_K) + \bar{g}_L \cdot (V - V_L)$.

Building upon the FitzHugh Nagumo model, Hindmarsh and Rose [64] proposed in 1984

a model (HR model) of neuronal activity described by three coupled first order differential equations:

$$\frac{dx}{dt} = y = 3x^2 - x^3 - z + I, \tag{1.16}$$

$$\frac{dy}{dt} = 1 - 5x^2 - y, \tag{1.17}$$

$$\frac{dz}{dt} = r \cdot (4(x + \frac{8}{5}) - z), \tag{1.18}$$

with $r^2 = x^2 + y^2 + z^2$, and $r \approx 10^{-2}$, so that the z variable changes very slowly. This extra mathematical variable allows for more dynamic behaviors for the membrane potential, described by the x variable of the model, by including the chaotic dynamics. This makes the Hindmarsh-Rose neuron model very useful to provide a good quantitative description of the many different patterns of the action potentials observed in experiments with relatively simple equations.

There are many other types of models that will not be listed here, for example, the Galves-Locherbach model(an inherently stochastic model to measure the probability that a given neuron i spikes in a time period t) and compartmental models to model cylindrically structured neurons. In general, for different purposes of research, models are selected and corrected accordingly to the question of biological interest.

As for the computational efficiency and biologically meaningfulness, Izhikevich [51] has summarized that the Integrate-and-Fire model has the smallest approximate number of floating point operations(FLOPS): FLOPS = 5, but is limited to tonic spiking, class 1 excitable and integrator. In contrast, the most complicated neuron is Hodgkin-Huxley with the number of FLOPS 1200, which is 240 times slower than the integrate-and-fire model. However, Hodgkin-Huxley neuron model is very biological meaningful, exhibiting a variety of robust neuron dynamics, including tonic spiking, phasic spiking, tonic bursting, phasic bursting, mixed mode, spike frequency adaptation, class 1 excitable, class 2 excitable, spike latency, sub-threshold oscillations, resonator, integrator, rebound spike, rebound burst, bi-

stability, DAP, accommodation, inhibition-induced spiking, inhibition induced burst and chaos.

1.3 Network dynamics

Scientists have identified some intrinsic neuronal properties that play an important role in generating membrane potential oscillations for a variety of neuron models. In particular, voltage-gated ion channels are critical in the generation of action potentials, as we have discussed in the last section about Hodgkin Huxley model. Also, the Integrate-and-Fire model is introduced for analytical proof on neural activities. Bifurcation analysis is one method that is often used by scientists to determine different oscillatory behaviors of the neuronal models, and make classifications of types of neuronal responses. Not only the periodic spiking, but also the sub-threshold membrane potential oscillations, for example, the resonance behavior that does not result in action potentials, may also contribute to oscillatory activity by facilitating synchronous activities of neighboring neurons. Like pacemaker neurons in central pattern generators, subtypes of cortical cells fire bursts of spikes rhythmically at preferred frequencies. Bursting neurons have the potential to serve as pacemakers for synchronous network oscillations, and bursts of spikes may underlie or enhance neuronal resonance [50].

In addition to intrinsic properties of spiking neurons, network properties are also crucial for oscillatory activities. Neurons communicate with one another through synapses and affect the spiking times in the post-synaptic neurons. Depending on the properties of the synaptic connection, such as the coupling strength, time delay and whether it is excitatory coupling or inhibitory coupling, the spike trains of the interacting neurons may become synchronized. Certain network structures promote oscillatory activities at some frequencies. For example, neuronal activities generated by two populations of interconnected inhibitory and excitatory spiking neurons can show spontaneous oscillations, which can be described by the Wilson-Cowan model.

Wilson and Cowan [65] has developed a set of integro-differential equations, forming a continuum model of cortex which demonstrated traveling waves, using the mean numbers of

activated and quiescent excitatory and inhibitory neurons,

$$\tau\frac{dE}{dt} = -E(t) + (1 - rE(t))f_E[w_{EE}E - W_{EI}I + h_E(t)], \tag{1.19}$$

$$\tau\frac{dI}{dt} = -I(t) + (1 - rI(t))f_I[w_{IE}E - W_{II}I + h_I(t)], \tag{1.20}$$

for the spatially homogeneous case, the equations are described as the following,

$$\tau\frac{\partial E(x,t)}{\partial t} = -E(x,t) + (1 - rE(x,t))f_E \tag{1.21}$$
$$(\int_{-\infty}^{\infty}\rho_E dx'\beta_{EE}(x-x')E(x',t) - \int_{-\infty}^{\infty}\rho_I dx'\beta_{EI}(x-x')I(x',t) + h_E(x,t)]),$$
$$\tau\frac{\partial I(x,t)}{\partial t} = -I(x,t) + (1 - rI(x,t))\prod f_I$$
$$(\int_{-\infty}^{\infty}\rho_E dx'\beta_{IE}(x-x')E(x',t) - \int_{-\infty}^{\infty}\rho_I dx'\beta_{II}(x-x')I(x',t) + h_I(x,t)]),$$

where ρ_E and ρ_I are, respectively, the packing densities of excitatory and inhibitory cells in the cortical slab and $E(x,t)$ and $I(x,t)$ are time coarse-grained,

$$E(x,t) = \int_{-\infty}^{t} dt'\alpha(t-t')n_E(x,t'), \tag{1.22}$$

$$I(x,t) = \int_{-\infty}^{t} dt'\alpha(t-t')n_I(x,t'), \tag{1.23}$$

where $n_E(x,t)$ and $n_I(x,t)$ are the proportions of excitatory and inhibitory neurons activated per unit time. $\alpha(t)$ acts as a low-pass filter.

The neural network forms through fast direct synaptic interactions between neurons. Also, oscillatory activity is modulated by neurotransmitters on a much slower time scale. That is, the concentration levels of certain neurotransmitters are known to regulate the amount of oscillatory activity. For instance, $GABA_A$ receptor densities have been shown to be positively correlated with frequency and negative correlated with amplitude of visually-induced gamma oscillations in human primary visual cortex (V1) [66]. The major neuro-

transmitter systems include the norepinephrine system, the dopamine system, the serotonin system, and the cholinergic system. These neurotransmitter systems affect the physiological state, e.g., wakefulness or arousal, and have a pronounced effect on amplitude of different brain waves, such as alpha activity [50].

At the single-cell level, the Integrate-and-Fire model captures most of the features of the dynamics of neurons, namely the voltage spike. Here, each neuron integrates input signals and generates an action potential when the membrane potential reaches a certain threshold of the neuron [13]

$$\sigma \frac{dV}{dt} = -V(t) + I(t) + \hat{V_R} \sum_n \delta(t - t_n), \tag{1.24}$$

where $V(t)$ represents the membrane potential at time t. $I(t)$ represents synaptic inputs which can be time-varying and location-varing. σ is the membrane time constant. If $V(t^-) = V_T$, the voltage threshold, then $V(t^+) = V_R$, the reset voltage, which is always less than the threshold voltage ($V_T > V_R$). This process is represented by the Dirac delta function or δ function,

$$\delta(t - t_n) = \begin{cases} 1, & \text{if } t - t_n = 0, \\ 0, & t - t_n \neq 0, \end{cases}$$

where t_n denotes the sequence of firing times of the neuron; that is, $V(t_n^-) = V_T$ for each $n > 1$. $\hat{V_R} = \sigma(V_R - V_T)$.

Synaptically coupled neurons transmit signals through the network. When a neuron sends a signal across a synapse, we call the sending neuron as the presynaptic cell and the receiving neuron as the postsynaptic cell. In the study of network dynamics, two components are crucial to our studies, one is the neuron model we select to use on the single-cell level, and the other is how the neurons are connected with one another. The total post-synaptic current to the i_{th} neuron can be expressed as following:

$$I_i(t) = \sum_j w_{ij} \sum_f \alpha(t - t_j^{(f)}), \tag{1.25}$$

where $t_j^{(f)}$ represents the time of the $f-th$ spike of the $j-th$ pre-synaptic neuron; w_{ij} is the strength of j synaptic efficacy between neuron i and neuron j [53]. Common choices for α include the instantaneous Dirac δ-pulse:

$$\alpha(t) = q\delta(t), \tag{1.26}$$

where q is the total charge injected into the synapses; the alpha synapse (Gerstner & Kistler (2002)),

$$\alpha(t) = \alpha\frac{t}{\tau}exp(1-\frac{t}{\tau}), \tag{1.27}$$

where α is a normalizing constant and τ is the time constant of the synapses.

In my research, the Integrate-and-fire model for a spiking neuron is mainly used for analytical solutions of activities of traveling wave propagation. The neuron spikes when the voltage reaches a certain threshold (V_T) and immediately it is reset to a lower voltage $V_R < V_T$. The effect of a spike on other neurons is to turn on a current whose time dependence is often a simple exponential function and whose magnitude is a function of the distance between the two connected neurons [31].

$$\tau_1\frac{\partial V(x,t)}{\partial t} = -V(x,t) + g_{syn}\int_D J(|y-x|)\sum_k \alpha(t-t_k(y))dy, \tag{1.28}$$

where $t_k(y)$ represents the discrete firing times when neuron at position y fires the k_{th} time. Here $\alpha(t)$ is the time-dependent current that arises from an impulse. The function Jdescribes the space dependence of the coupling strength of neuron at position x and y. The parameter g_{syn} sets the global scale of the coupling strength.

$$J(x) = \frac{e^{-|x|/\sigma}}{2\sigma}, \tag{1.29}$$

$$\alpha = e^{-t/\tau_2}H(t). \tag{1.30}$$

H is the Heaviside step function

$$H(t) = 0, t < 0$$

$$H(t) = 1, t \geq 0.$$

Osan et. al [34] has obtained the integral formulation of the Integrate-and-Fire neural model by integrating the differential equation 1.28,

$$V(x,t) = \sum_{n=1}^{N(x,t)} \eta(t - t_n(x)) + g_{syn} \int_D J(|y-x|) \sum_{m=1}^{N(y,t)} A(t - t_k(y))dy, \tag{1.31}$$

$$\eta(t) < -(V_{reset} - V_T)e^{-t/\tau_1}H(t), \tag{1.32}$$

$$A(t) = \frac{1}{1-\tau_1/\tau_2}(e^{-t/\tau_2} - e^{-t/\tau_1})H(t) = \frac{\alpha(t) - \beta(t)}{1-\tau_1/\tau_2}, \tag{1.33}$$

where $\beta(t) = e^{-t/\tau_1}H(t)$. We call $\alpha(t)$ 'decaying reset', and $\beta(t)$ 'synaptic integral'. The following Figure 1.2 visualized the fast and slow response curve function: $A(t)$ regarding to different parameter settings. $V(x,t)$ equals V_T when the neuron spikes.

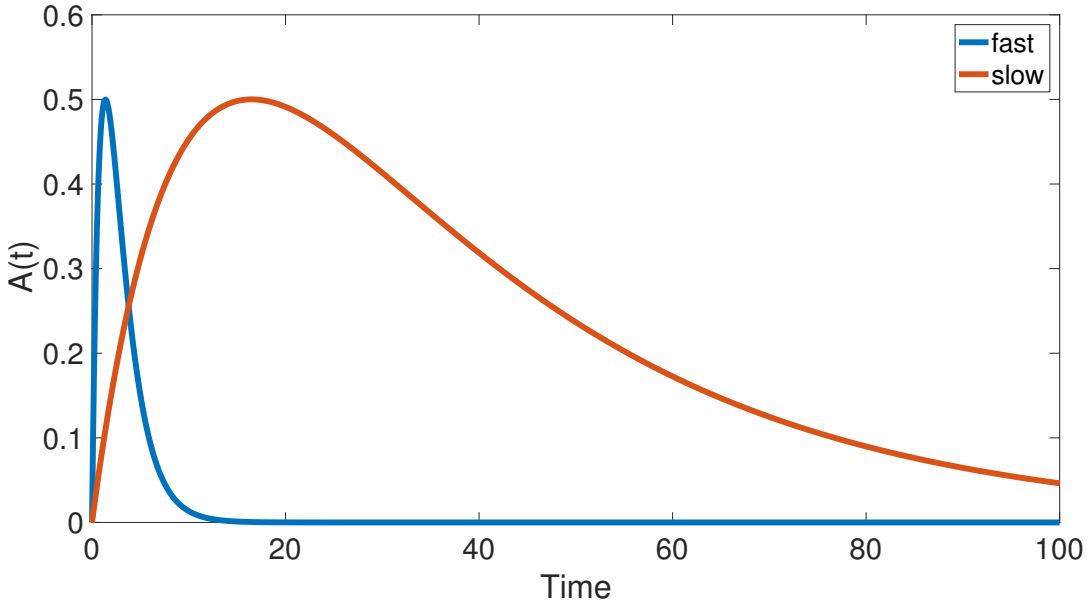

Figure (1.2) **Fast and slow response functions, $A(t)$ with different τ_1 and τ_2, regenerated the work by Osan et. al [34]**

Fast and slow response functions, $A(t)$ with $\tau_1 = 1$, $\tau_2 = 2$ for the fast one(blue line) and $\tau_1 = 10$, $\tau_2 = 30$ for the slow one(red line). Note the heights have been normalized here to be the same.

Osan and Ermentrout [34] have used a discretized one-dimensional domain. They applied a uniform grid with distance δ between nodes. By denoting spatial position of each neuron by $x = i\delta$, where i is the numbering of each neuron. Under the assumption that each neuron makes a single spike, they integrate the equations to obtain the following integral equation for $V(x,t)$ using $V(0,0) = 0$ in discrete and continuous forms [31]:

$$V(i,t) = g_{syn}\delta \sum_{j=1}^{\inf} J(|i-j|\delta)A(t-t_j), \tag{1.34}$$

$$V(x,t) = g_{syn} \int_D J(y-x)A(t-t_y)dy. \tag{1.35}$$

Besides, multiple-spikes traveling waves are also analytical tractable similar to single-

spike traveling wave but excitations are coming from integration or summation from more than one neighbor neurons' spiking.

$$V(i,t) = g_{syn}\delta \sum_{k=1}^{\inf} J(|i-j|\delta) \sum_{m=1}^{N(k,t)} A(t - t_m(k)), \tag{1.36}$$

$$V(x,t) = g_{syn} \int_D J(y-x) \sum_{m=1}^{N(k,t)} A(t - t_y)dy. \tag{1.37}$$

Furthermore, two-dimensional integrate-and-fire neural network evolution equations have also been brought up on single-spike traveling waves [36]. The time at which the neuron fires, $t^*(x)$ is defined to be the first time for which $V(x,t)$ reaches threshold V_T. With radially symmetric solutions, the two-dimensional evolution equation is,

$$V(r,t) = \int_0^{\infty} \hat{J}(r,r')A(t^*(r) - t^*(r'))dr' \tag{1.38}$$

where

$$\hat{J}(r,r') = r' \int_0^{2\pi} J(\sqrt{r^2 + r'^2 - 2rr'cos(\theta)})d\theta \tag{1.39}$$

Those forms of evolutions equations for traveling wave propagation activities are very powerful to obtain analytical results from the propagation activities of traveling waves. They can also be extended to more complicated cases when the coupling function is not exponential function and it is a non-homogeneous neural network. The research questions are: Can we obtain traveling wave speed solutions and prove that there exist two traveling wave speeds: slow-unstable and fast-stable? Can we obtain explicit expressions for traveling wave propagation activities related with speed, acceleration, neuron locations, spiking times, and network parameters: synaptic global excitability, neuron integration time constant, neuron synaptic excitation decay time constant, neuron connectivity spatial scale? What are the dynamics when the integrate-and-fire neural network is under the influence of periodic inhomogeneities?

Traveling waves of electrical activities, due to neurons interaction, have been observed in vivo in various sensory cortical areas. The emergence of this type of traveling waves is a characteristic feature of some neurological disorders in human, such as epilepsy and migraines. As discussed in the section of 'Motivations' about why we study the traveling waves of electrical activities, here I will describe how this type of traveling waves is usually recorded. A common experimental method to record electrical activity in vitro is to use thin slices of cortical tissue, which is typically considered as a reduced one-dimensional network in mathematical analysis. In the preparation of the recording, inhibition is suppressed by blocking $GABA_A$ receptors with an antagonist such as bicuculline [67]. A weak electrical stimulus from any site on the cortical slice can induce a synchronization of electrical activities. Then the traveling wave can propagate away from the stimulate point at a mean speed around 6-9 cm/s.

Under the assumption that the synaptic coupling between neurons are homogeneous, it has been shown that an excitatory neural network supports the propagation of a traveling wave front by Ermentrout, Abbott, Bressloff, Folias and Golomb ([13], [30], [52], [68]). Also, periodic inhomogeneity is found in the primary visual cortex that the horizontal connections rotates approximately periodically across the cortex resulting in a periodic inhomogeneous medium. Bressloff [45] derived an expression for the effective wave-speed and showed that propagation failure could occur if the speed is too slow or the degree of inhomogeneity is too large using averaging and homogenization theory. Kilpatrick, Folias and Bressloff [47] continued the work on the traveling pulses and wave propagation failure in inhomogeneous neural media using averaging and homogenization theory. They have shown that a spatially periodic modulation of homogeneous synaptic connections leads to an effective reduction in the mean speed of a traveling pulse. The bumps at the leading edge of the pulse are also found as a feature of coherent traveling wave propagation. Here is the one-dimensional

neural network model,

$$\frac{\partial u(x,t)}{\partial t} = -u(x,t) + \int_{-\infty}^{\infty} W(|x-x'|)[1 + D'(\frac{x'}{\epsilon})]f(u(x',t))dx' - \beta v(x,t),$$
$$\frac{1}{\alpha}\frac{\partial v(x,t)}{\partial t} = -v(x,t) + u(x,t),$$

where D is a $2\pi-$periodic function and ϵ determines the microscopic length-scale. W is the homogeneous weight function or coupling function. $f(u)$ is the output firing rate function. $v(x,t)$ is a local negative feedback mechanism, with β and α determining the relative strength and rate of feedback. $u(x,t)$ is the population activity at position x.

By the assumption that ϵ is a small parameter and the homogeneous network supports the propagation of a traveling pulse of constant speed c.

$$u(x,t) = U(\xi),$$
$$v(x,t) = V(\xi),$$

where $\xi = x - ct$, and $U(\xi), V(\xi) \to 0$ if $\xi \to \pm\infty$. By substituting x, t by ξ and performing the change of variables ($\xi = x - \phi(t)$) and $\tau = t$, the model is described in the following form,

$$\frac{\partial u(\xi,\tau)}{\partial \tau} = -u(\xi,\tau) + \int_{-\infty}\infty W(\xi-\xi')f(u(\xi',\tau))d\xi' + \phi'\frac{\partial u(\xi,\tau)}{\partial \xi}$$
$$+\epsilon\int_{-\infty}^{\infty} D(\frac{\xi'+\phi}{\epsilon})[W'(\xi-\xi')f(u(\xi',\tau)) - W(\xi,\xi')\frac{\partial f(u(\xi',\tau))}{\partial \xi'}d\xi',$$
$$\frac{1}{\alpha}\frac{\partial v(\xi,\tau)}{\partial \tau} = -v(\xi,\tau) + u(\xi,\tau) + \frac{\phi'\partial v(\xi,\tau)}{\alpha\partial\xi}.$$

By performing the perturbation expansions on the voltage $U(\xi), V(\xi)$ and speed c,

$$u(\xi,\tau) = U(\xi) + \epsilon u_1(\xi,\tau) + \epsilon^2 u_2(\xi,\tau) + ...,$$
$$v(\xi,\tau) = V(\xi) + \epsilon v_1(\xi,\tau) + \epsilon^2 v_2(\xi,\tau) + ...,$$
$$\phi'(\tau) = c + \epsilon\phi_1'(\tau) + \epsilon^2\phi_2'(\tau) + ...$$

where $(U(\xi), V(\xi))^T$ is a traveling pulse solution of the corresponding homogeneous system and c is the speed of the unperturbed pulse. It is shown [47] that there exists a traveling pulse of the approximate form $U(x - \phi(t))$ and of average speed $\bar{c} = 2\pi\epsilon/T$ with

$$T = \int_0^{2\pi\epsilon} \frac{d\phi}{c - \epsilon\Phi_1(\phi/\epsilon)}$$

1.4 Numerical Computing with MATLAB

Apart from the analytical methods, it is important to numerically simulate the system of neural networks to confirm analytical results and provide insights on implicit results from the neural models. Ordinary differential equation (ODE) solver in Matlab is very helpful for numerical simulation of traveling wave spiking activities since the integrate-and-fire model is mainly a system of ordinary differential equations of voltage with respect to time and neuron locations after making transformations.

In Matlab, there are several types of ODEs, for example, ODE45, ODE23, ODE113, ODE15s. Among them, ODE45 and ODE15s are the most frequently used in my Ph.D. research to solve differential equations. ODE45 is based on an explicit Runge-Kutta (4, 5) formula, the Dormand-Prince pair, it is a single-step solver in computing $y(t_n)$, it needs only the solution at the immediately preceding time point, $y(t_{n-1})$. It is a quite efficient solver. However, it is a non-stiff differential equation solver.

ODE15s is based on the numerical differentiation formulas (NDFs) of orders 1 to 5. It is a variable-step, variable-order (VSVO) solver. Optionally, it can use the backward differentiation formulas (BDFs, also known as Gear's method) that are usually less efficient. It is generally used for stiff problems. General Matlab code is put here,

$$[X, T] = ode**(@F, TimeSpan, x_0, Options, P1, P2, P3), \tag{1.40}$$

where $@F$ is a handle to a function which returns a vector of rates of change. x_0 is the timespan in a vector form $[start, end]$. We can use $Options$ to set various options associated

with the ode solver (if omitted or set to [], the default settings are used). $P1, P2, P3$ are additional arguments which will be passed to $@F$.

Additionally, the model is basically described as non-linear equations. Numerically, we use $fsolve, fminbnd, lsqnonlin, fzero$ to help us get solutions from 2-D or n-D nonliear systems to confirm the analytical results of traveling wave propagation activities. $fsolve$ solves systems of nonlinear equations with given initial conditions. However, $fsolve$ cannot include any constraints, even bound constraints. In this case, we need $fminbnd$ and $lsqnonlin$. $lsqnonlin$ tries to minimize the sum of squares of the components of a vector function $F(x)$, which attempts to solve the equation $F(x) = 0$ with constraints settings.

CHAPTER 2

ACTIVITIES OF TRAVELING WAVE PROPAGATION IN HOMOGENEOUS NUERAL TISSUE

2.1 Evolution equations in integrate-and-fire model

In this study we seek analytical solutions for evolution of one-spike activity propagation in a class of neural networks. Here we use a simple and widely used model for a spiking neuron, the integrate-and-fire model, which integrates the input signal with temporal constant τ_1 until its voltage reaches a threshold V_T, at which point the neuron sends an excitatory spike to the rest of the network.

$$V(x,t) = g_{syn} \int_D J(x,y) A(t - t^*(y)) dy. \tag{2.1}$$

To describe the network interactions we make use of the following two functions. First, $J(x,y)$ describes the synaptic coupling between neurons at positions x and y. Second, $A(t)$ describes the excitation provided by a presynaptic spike onto the postsynaptic neuron. The functions $J(x,y)$ and $A(t)$ take the following explicit form:

$$J(x,y) = \frac{e^{\frac{-|x-y|}{\sigma}}}{2\sigma}, \tag{2.2}$$

$$A(t) = \frac{e^{-\frac{t}{\tau_2}}}{1-\frac{\tau_1}{\tau_2}} - \frac{e^{-\frac{t}{\tau_1}}}{1-\frac{\tau_1}{\tau_2}} = A_2(t) - A_1(t), \tag{2.3}$$

where

$$A_1(t) = \frac{e^{-\frac{t}{\tau_1}}}{1-\frac{\tau_1}{\tau_2}},$$

$$A_2(t) = \frac{e^{-\frac{t}{\tau_2}}}{1 - \frac{\tau_1}{\tau_2}}.$$

For function $J(x, y)$, which depends only on the absolute value of $|x - y|$, the symbol σ indicates the connectivity spatial scale. Other explicit functions for $J(x, y)$ will be considered later on. For the temporal function $A(t)$, τ_2 is the time constant for the decay of the synaptic excitation which is assumed to be greater than τ_1; also $A(t) = 0$ for $t < 0$. The membrane voltage for a neuron in the network then can be expressed in integral form [31]:

$$\frac{V(x,t)}{g_{syn}} = J \otimes A = \int_{-\infty}^{x} J(x,y)A(t - t(y))dy \tag{2.4}$$

where $\otimes$ denotes convolution and $t(y)$ is the spiking time for the neuron at position y.Here g_{syn} is a constant that controls the excitation of the network. It is assumed that dynamics in the network are completely determined by the excitation due to the previous neuron spikes that occur at $t(y) < t$. We note here that initiation of activity propagation may initially occur through applying an external current to a subset of neurons in the network. For example a preferred way to do this in the numerical simulation is to induce a large group of neurons to spike at the same time, $t = 0$, and then to monitor propagation to the right of that region. For simplicity we assume that the wave propagates only in one direction, taken here to be from left to right, and we ignore neural spikes that may occur to the left of the initiation region. After integrating the excitatory signals, the firing condition of a neuron at position x, taken to be at the leading edge of the propagation, becomes $V(x, t(x)) = V_T$. Since $t(x)$ is the time at which the voltage $V(x, t)$ of neuron at position x first crosses threshold, this constitutes a consistency equation. In this one-dimensional network, it can be shown that the firing time is a monotonic function of their position x; this holds true for many other classes of connectivity functions [33, 34]

We take two derivatives of equation (2.4) with respect to x, with the goal of obtaining an equation that connects $t' = dt/dx$ and $t'' = d^2t/dx^2$ which represent an inverse of speed and a transformation of acceleration. For the first derivative of equation (2.4), the left side

is a constant and becomes 0 after first derivative.

$$\frac{d(V_T/g)}{dx} = (J \otimes A)' = J' \otimes A + (J \otimes A')t' = 0. \tag{2.5}$$

$$0 = J'' \otimes A + 2t'J' \otimes A' + t''J \otimes A' + (t')^2 J \otimes A'' + J_0 A_0' t'. \tag{2.6}$$

where we used $A_0 = A(x = 0) = 0$ in equations (2.6). The other notations used here are:

$$J_0 = J(0) = 1/2/\sigma.$$

$$A_0' = A'(0) = 1/\tau_1.$$

Equations (2.4-2.6) constitute a system of evolution equations that shape the traveling wave propagation which containing t' and t''.

In the next section we will show how we can convert them to an ordinary differential equations that could describe the traveling wave speed and acceleration.

2.2 Analytical solutions

Since functions $J(x)$, $A_1(t)$ and $A_2(t)$ are all exponentials, the system of equations (2.4-2.6) contains only two unknowns, of the form

$$K_1 = J \otimes A_1.$$

$$K_2 = J \otimes A_2.$$

Solving for them as a function of t' in the equations (2.4-2.5) and substituting these solutions in (2.6) yields an equation where t'' is a function of t'. This is the plan.

Also by the fact that $J(x), A_1(t)$ and $A_2(t)$ are exponential functions, we obtain: $J' = \frac{dJ(x)}{dx} = J/(-\sigma), A'_k = \frac{dA_k(t(x))}{dx} = A_i/(-\tau_k)t', k = 1, 2$. Then we can write equations (2.4-2.5) in a compact way:

$$\frac{V_T}{g_{syn}} = K_2 - K_1. \tag{2.7}$$

$$K_2(\frac{1}{\sigma} + \frac{1}{\tau_2}t') = K_1(\frac{1}{\sigma} + \frac{1}{\tau_1}t'). \tag{2.8}$$

Terms K_1 and K_2 can now be determined from equations (2.7-2.8) as functions of the instantaneous speed $c = 1/t'$. By substitution,

$$(\frac{V_T}{g_{syn}} + K_1)(\frac{1}{\sigma} + \frac{1}{\tau_2}t') = K_1(\frac{1}{\sigma} + \frac{1}{\tau_1}t')$$

Thus, we can solve for K_1 and obtain K_2 through back-substitution. Here are the solutions,

$$K_1 = \frac{V_T}{g_{syn}}(\frac{c}{\sigma} + \frac{1}{\tau_2})/(\frac{1}{\tau_1} - \frac{1}{\tau_2}) \tag{2.9}$$

$$K_2 = \frac{V_T}{g_{syn}}(\frac{c}{\sigma} + \frac{1}{\tau_1})/(\frac{1}{\tau_1} - \frac{1}{\tau_2}) \tag{2.10}$$

Actually K_2 is a multiple of K_1 (Fig. 2.1).

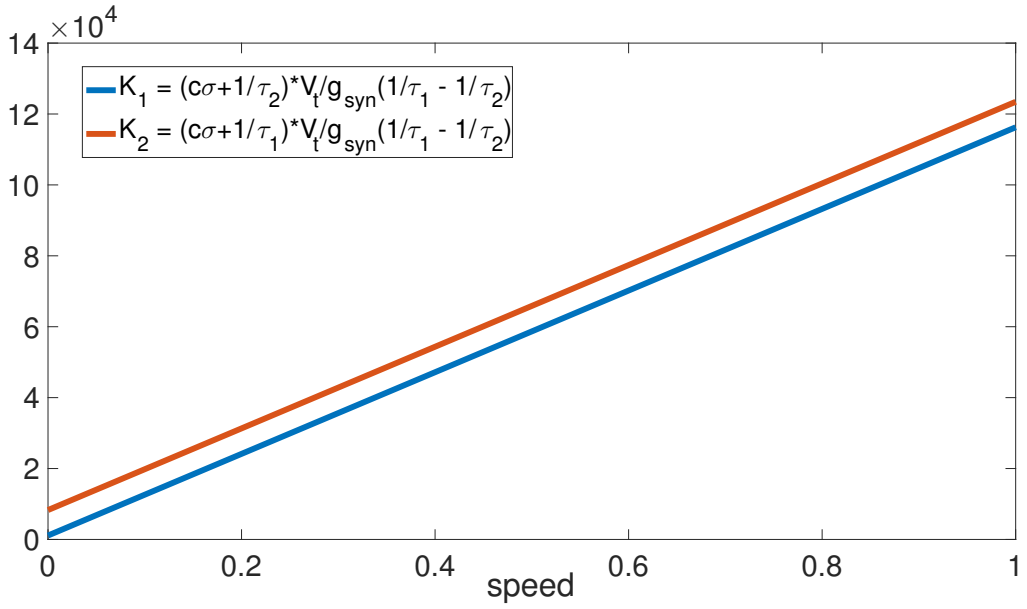

Figure (2.1) K_1 **and** K_2 **linearly change over speed.**

K_1 and K_2 from equations 2.7-2.8 are multiples of each other. They are linearly correlated with speed. These analytical results are also used in the inhomogeneous neural network.

In order to get speed and acceleration related equation, we can rewrite equation (2.6) by taking the second derivative as a single equation that relates t'' to c:

$$\frac{d^2t_x}{dx^2} = \frac{K_1(\frac{1}{\sigma} + \frac{1}{c\tau_1})^2 - K_2(\frac{1}{\sigma} + \frac{1}{c\tau_2})^2 - \frac{1}{2\sigma c\tau_1}}{\frac{K_1}{\tau_1} - \frac{K_2}{\tau_2}} \tag{2.11}$$

Substituting the explicit solutions for the terms K_1 and K_2 in equation (2.11), we can determine d^2t_x/dx^2 as a function of speed, which is

As an additional step, we convert d^2t_x/dx^2 into the instantaneous acceleration, which is a more intuitive measure for the activity propagation, using the following relationship

between these two quantities:

$$a(x) = \frac{d^2x}{dt_x^2} = -\frac{1}{(\frac{dt_x}{dx})^2}\frac{d^2t_x}{dx^2}\frac{dx}{dt_x} = -c^3\frac{d^2t_x}{dx^2}. \tag{2.12}$$

Thus by substitution with,

$$\frac{d^2t_x}{dx^2} = -\frac{a(x)}{c^3}. \tag{2.13}$$

We obtain a remarkably simple analytical relationship between $a(x)$ and $c(x)$:

$$a(x) = -\frac{(c(x) - c_1)(c(x) - c_2)}{\sigma} \tag{2.14}$$

where c_1 and c_2 are the speed for the slow-unstable and the fast-stable constant speed traveling wave solutions respectively. By solving for $c(x)$,

$$-\frac{(c(x) - c_1)(c(x) - c_2)}{\sigma} = 0$$

We obtain two speed solutions,

$$c_{1,2} = \sigma/2\Big(B - \beta \mp \sqrt{(B-\beta)^2 - \frac{4}{\tau_1\tau_2}}\ \Big) \tag{2.15}$$

These constant speed wave solutions(c_1 and c_2) depend on parameters σ, τ_1, τ_2 and $B = g_{syn}/(2V_t\tau_1), \beta = (\tau_1+\tau_2)/(\tau_1\tau_2)$, which we also have the visualization(FIG. 2.2a). c_1 and c_2 are separately unstable and stable constant speed solutions, which means that propagation will decrease all the way to zero if the speed is less than c_1 and when the speed is above c_1, the propagating speed will converge to c_2 as we say 'stable'. With parameters values: $\tau_1 = 4 \times 10^{-3}$, $\tau_2 = 3.0 \times 10^{-2}s$, $\sigma = 2.88 \times 10^{-4}m$, $V_T = 1.5 \times 10^{-2}V$, $g_{syn} = 9.84 \times 10^{-2}V$, we have $c_1 = 4.6 \times 10^{-3}m/s$ and $c_2 = 1.500 \times 10^{-1}m/s$.

The pair of speeds, c_1 and c_2 are supposed to be real and positive for different values of network excitability g_{syn}, provided that this parameter exceeds a critical value $g_{critical}$ (FIG. 2.2b), which gives the minimum synaptic strength for which stable activity propagation can exist:

$$g_{critical} = 2V_t\tau_1\left(\frac{\tau_1+\tau_2}{\tau_1\tau_2} + \sqrt{\frac{4}{\tau_1\tau_2}}\right) \tag{2.16}$$

This critical g_{syn}(the minimum global excitability for traveling wave propagation) is positively correlated with the integration time constant (τ_1) and negatively correlated with the excitation decay time constant (τ_2)(Fig.2.3)(a-b).

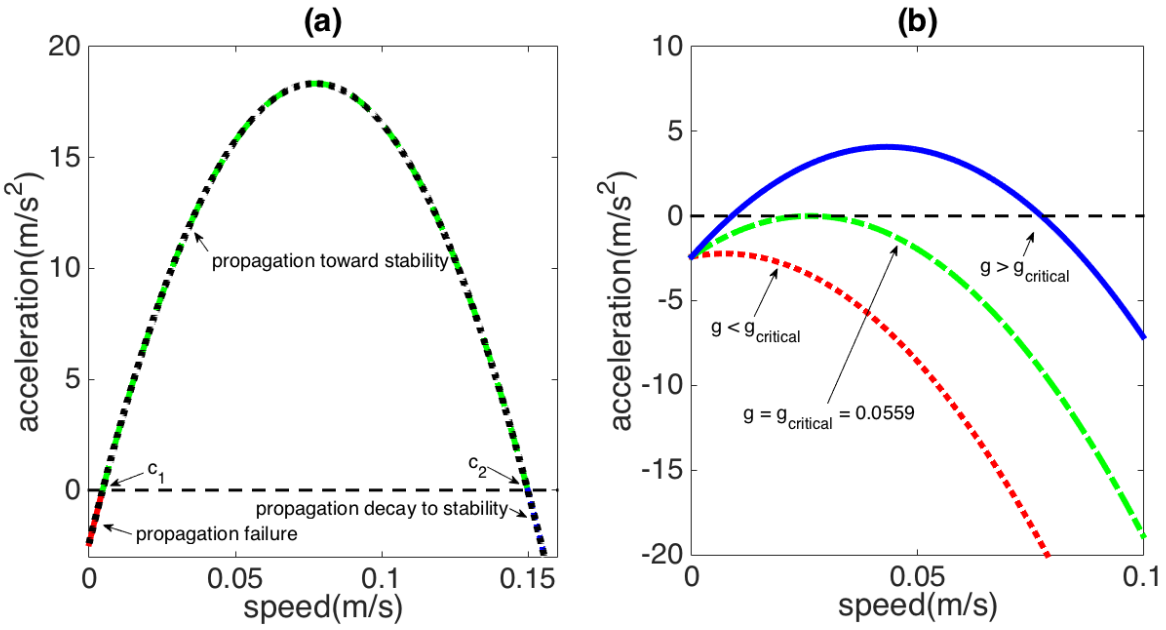

Figure (2.2) **(a) Theoretical results and numerical simulations for the dependence of wave acceleration on instantaneous speed,** $a = a(c)$**.** The acceleration's quadratic dependence on speed (curve with merged blue, green and red regions) is in perfect agreement with numerical simulations (dotted black line) on all regions with exception of low speed regime where the agreement again becomes excellent with finer discretization of the spatial domain. The parameters used here are: $\tau_1 = 4 \times 10^{-3}$, $\tau_2 = 3.0 \times 10^{-2}s$, $\sigma = 2.88 \times 10^{-4}m$, $V_T = 1.5 \times 10^{-2}V$, $g_{syn} = 9.84 \times 10^{-2}V$, yielding $c_1 = 4.6 \times 10^{-3}m/s$ and $c_2 = 1.500 \times 10^{-1}m/s$. These parameters are in agreement with published data and they are used as default values, unless noted otherwise. **(b) Theoretical results for acceleration vs speed for different excitability levels** g_{syn}**.** Depending on the overall excitability level, there are no traveling wave solutions (red line), one solution (green line) or two solutions (blue line). As excitability increases, c_1 and c_2 decrease or increase respectively, provided that the overall excitability exceeds the critical value $g_{critical} = 0.0559V$ (see Eq. 2.16).

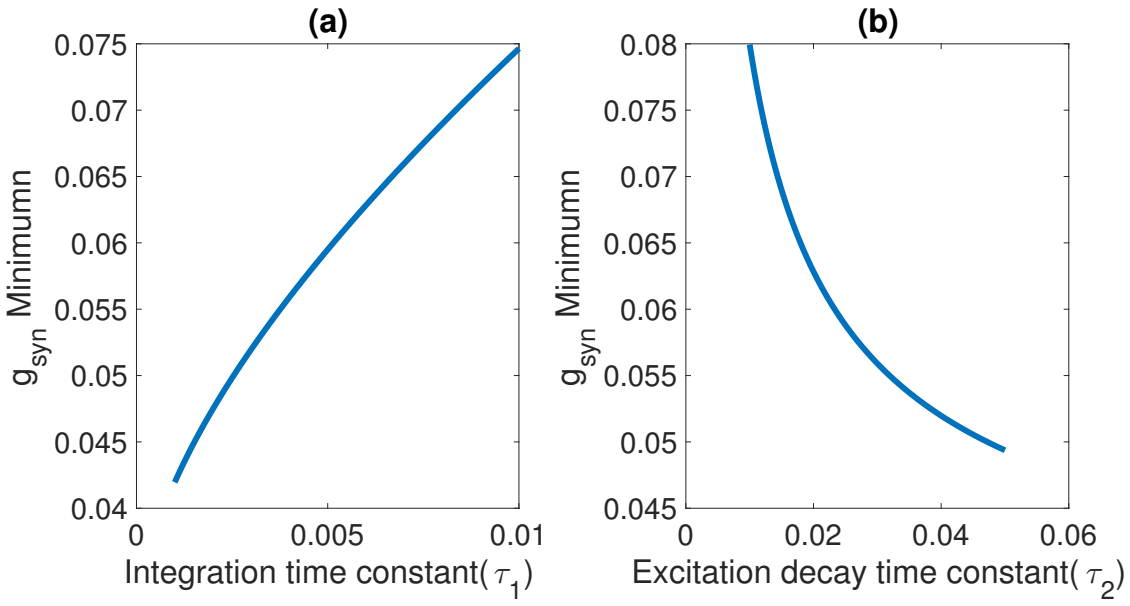

Figure (2.3) **Minimum global excitability(g_{syn}) over τ_1, τ_2.**

(a). g_{syn} vs τ_1. The minimum global excitability required for traveling wave propagation increases with the increase of integration constant time. (b). g_{syn} vs τ_2. The minimum global excitability required for traveling wave propagation decreases with the increase of excitation decay constant time.

In agreement with previous results, the decrease of the excitability parameter g_{syn} brings the two solutions c_1 and c_2 closer and closer together, until these solutions collide and cease to exist. Below $g_{critical}$, c_1 and c_2 become complex, and in turn, the acceleration can only take negative values, resulting in eventual propagation failure regardless of how activity propagation is initiated. This relationship is evident in FIG. 2.4a, where the connection between $c_{1,2}$ and g_{syn} is illustrated. The slow-unstable wave has a horizontal speed asymptote at zero as g_{syn} goes to ∞, while the fast-stable wave has a oblique asymptote with slope σB. The same properties exhibited by equation (2.15) were found numerically [29], in agreement with later results [30, 32]. The dependence of the c_1 and c_2 on other network parameters such as connectivity footprint σ, the neuron integration time τ_1 and the decay time of synaptic excitation τ_2 is illustrated in FIG. 2.4b-d. We can find that the higher global excitability increases wave propagation speed and become more linear when g_{syn} increases.

The connectivity footprint σ reveals a linear correlation with propagating speed. Also, the constant speed solution will decrease if the integration time increase which means the integration is less slow, While with the decay time increases (τ_2), meaning the voltage is decreasing slower, the stable speed(c_2) will be larger, but there is a limit stable speed that the neural network can reach to.

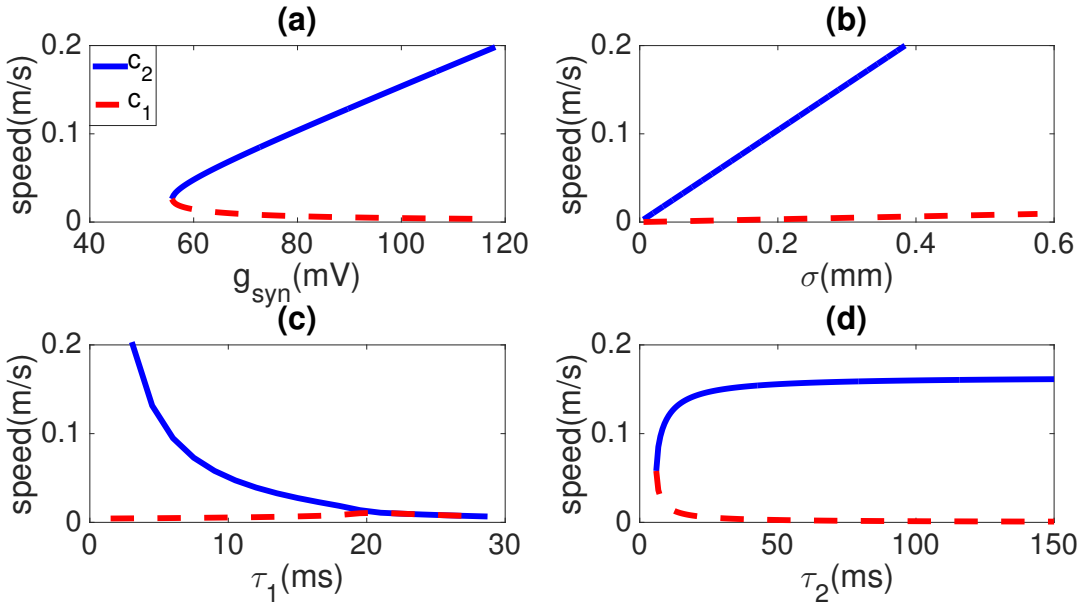

Figure (2.4) **Dependence of traveling wave solutions c_1 (in red) and c_2 (in blue) on neuron and network parameters.** **(a) Speed vs synaptic excitability** g_{syn}, with bifurcation occurring at $g_{critical} = 55.9mV$. **(b) Speed vs** σ, revealing linear correlations between propagating speed and parameter σ. **(c) Speed vs** τ_1, showing a decrease of c_2 as the neuron integration time, τ_1, increases. **(d) Speed vs** τ_2, indicating that fast solutions increase with the increase of decay time, τ_2, in contrast to the slow solutions showing the opposite trend.

A consequence of the relationship between acceleration and speed (Eq. 3.7) is that the traveling waves fails if $c < c_1$ or evolves toward $c(\infty) = c_2$ if $c > c_1$. These outcomes are illustrated in FIG. 2.5a, which shows the neuronal positions versus their firing times. As a reminder, activity propagation is initiated here by inducing a large enough region to spike at

$t = 0$ through the application of a large enough external current to all neurons in that region. The size of the initial region, which needs to exceed a threshold value, allows us to control the initial phase of the traveling wave, as larger regions will provide more excitation to the neurons close to the initiation region and it will consequently result in a larger initial speed for the activity propagation. In order to have stable constant wave propagation, solutions are assumed to be real, thus

$$(B - \frac{\tau_1 + \tau_2}{\tau_1 \tau_2})^2 - \frac{4}{\tau_1 \tau_2} > 0. \tag{2.17}$$

Not surprisingly, when we examine the evolution of speed as a function of space (FIG. 2.5b), we notice again the existence of three distinct regimes in agreement with our previous results:

- propagation failure if $c < c_1$,
- Acceleration toward stable speed c_2 if $c > c_1$,
- Deceleration toward stable speed c_2 if $c > c_2$.

From Figure 2.5a-b, we also can conclude that propagation failure can be achieved in a finite amount of space, while the stability at c_2 can be achieved asymptotically. In the next section, we will discuss about the coupling between speed and acceleration and explicit equations for firing times and space with respect to speed and other parameters.

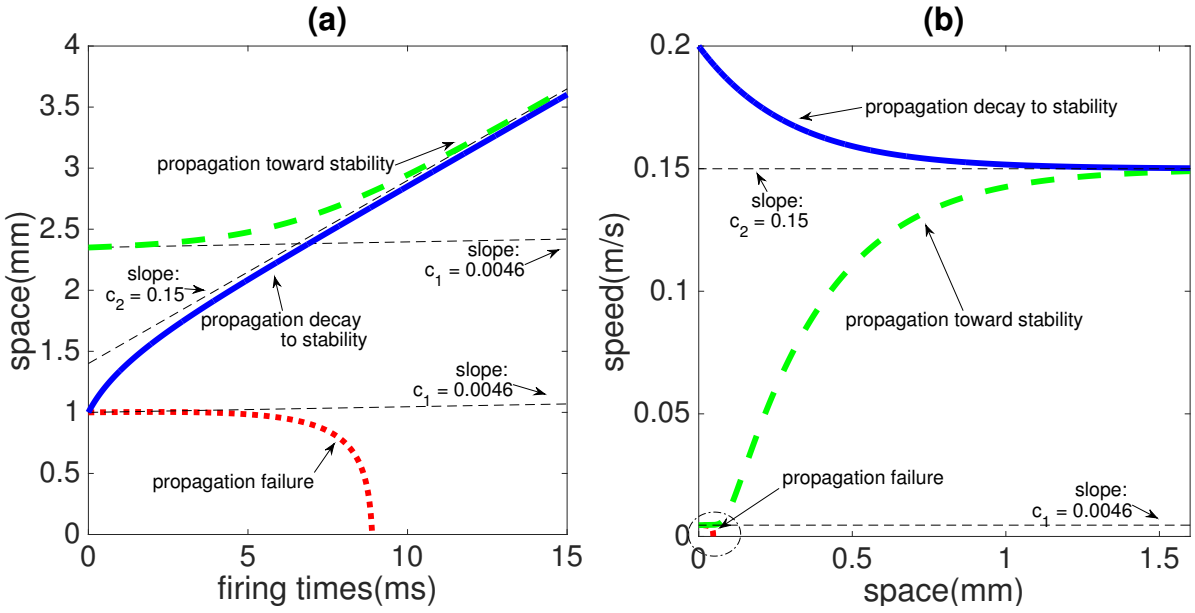

Figure (2.5) **(a) Space vs Firing times.** Different initial conditions will determine if the transients evolve toward stable or transient propagation. When the speed (tangent) is less than c_1, propagation fails as expected (red line, failure when tangent becomes vertical). When the tangent is greater than c_2 (blue line), the traveling wave slows down and evolves asymptotically toward the a constant speed traveling wave indicated by slope c_2. When the tangent is greater than c_1 but less than c_2 (green line), the traveling wave speeds up and evolves asymptotically toward fast-stable solution at c_2. Results from numerical simulations, not shown here, are in perfect agreement with color lines shown in this graph. **(b) Speed vs Space.** In agreement with results from part (a), propagation failure is achieved in a finite amount of space, while stability at c_2 is achieved asymptotically.

2.2.1 Coupling between speed and acceleration leads to wave stability

Most surprisingly, equation (3.7) reveals that the relationship between the acceleration and the instantaneous speed is independent of how the wave was initiated. More precisely, any two instances of activity propagation that achieve the same speed will follow the same future dynamics despite the fact that the prior firing maps are different.

This is not a trivial result, since in principle each spike in the network exerts an influence

on the rest of the network, so the naive intuition would be that different initial conditions would result in activity propagation dynamics, even for the cases of speed-matching at a common point in the network.

We can see from FIG. 2.2a that the two roots of the quadratic equation correspond to the constant low speed unstable and high speed stable traveling wave solutions. This provides a global stability explanation for why any transient propagation will evolve toward a constant speed solution with speed c_2, provided that the initial speed of the propagation is larger than c_1, or fail otherwise. When $c < c_1$ acceleration stays negative and increases in amplitude as the wave slows down toward propagation failure at $c = 0$. When $c_1 < c < c_2$ acceleration stays positive but decreases in amplitude as the wave speeds up toward the constant speed solution with $c = c_2$. When $c > c_2$ acceleration stays negative but decreases in amplitude as the wave slows down toward the constant speed solution with $c = c_2$.

All these trends are true regardless of the exact value of initial speed c, therefore these results go beyond typical proofs of stability for traveling waves, which are usually done using perturbation theory [29,69], meaning that the results hold only for small perturbation around the stable constant speed traveling wave. In contrast, our stability argument holds for random shuffling of firing times or perturbations of arbitrary large amplitude in voltage, and as such are more general in nature than the ones resulting from the perturbation theory.

2.2.2 Analytical solutions and natural timescales for activity propagation

We now take advantage of this remarkable result from equation(2.14) to determine analytical expressions for $t(x), c(t), x(t)$ and $x(c)$ by variable separation and taking derivations with respect to the parameter that is of interest. In this case, it helps us understand the mathematic form of characteristics of traveling wave propagation, like spiking time, propagating speed, space distance that traveled. Since we have the form of ordinary differential equation for speed, acceleration of space distance(2.14), we can perform different integrations by the relationship between speed, space distance and traveling time.

With the fact that,

$$a = \frac{dx}{dt}\frac{dc}{dt}$$

We can rewrite (3.7) into the form as following,

$$c\frac{dc}{dt} = -\frac{(c-c_1)(c-c_2)}{\sigma}.$$

This is a nice ordinary differential equation and the only trouble to analytical solutions($c(x)$) comes from the term $(c-c_1)(c-c_2)/c$. However, we can get analytical expressions for the forms like $t(x), c(t), x(t)$ and $x(c)$.

Integrating equation (3.7) after separating variables c and t by the following steps,

$$dt = -\frac{\sigma c}{(c-c_1)(c-c_2)},$$

$$\int_0^t dt = -\sigma \int_{c(0)}^{c(t)} \frac{c}{(c-c_1)(c-c_2)} dc.$$

With the trick to separate the right quadratic term in the denominator into one linear term to perform integration,

$$\frac{c}{(c-c_1)(c-c_2)} = \frac{-c_1}{c_2-c_1}\frac{1}{c-c_1} + \frac{c_2}{c_2-c_1}\frac{1}{c-c_2}.$$

As expected, we obtain

$$t(c) = \frac{\sigma}{c_2-c_1}\ln(\frac{c-c_1}{c-c_2}k), \tag{2.18}$$

where $k = (c_0 - c_2)/(c_0 - c_1)$ and c_0 is the initial propagation speed at $t = 0$,

$$t(c_0) = \frac{\sigma}{c_2 - c_1} \ln\left(\frac{c_0 - c_1}{c_0 - c_2}\frac{c_0 - c_2}{c_0 - c_1}\right) = 0.$$

From this analytical result, we can see that the firing time changes in a logarithmic form with respect to the *speed* change, which is in agreement with our previous figures.

Similarly, inverting $c(t)$ in equation (2.18) and using the definition $\tau_0 = \sigma/(c_2 - c_1)$ we obtain:

$$e^{t/\tau_0} = k\frac{c - c_1}{c - c_2}.$$

Thus,

$$c(t) = \frac{c_2 e^{t/\tau_0} - c_1 k}{e^{t/\tau_0} - k}. \tag{2.19}$$

Integrating both equations of (2.19) since $c(t) = dx/dt$ after separating variables x and t,

$$x(t) = \sigma \ln\left(\frac{e^{t/\tau_0} - k}{e^{t_0/\tau_0} - k}\right) + c_1(t - t_0). \tag{2.20}$$

where t_0, which in general is different from 0, is the firing time of neuron located at position $x = 0$. In order to relate the speed of propagation with the spatial position, we take the integral of equation (3.7) after separating variables x and c, also using $a(x) = c \cdot dc/dx$:

$$x(c) = \tau_0(c_1 \ln\left(\frac{c - c_1}{c_0 - c_1}\right) - c_2 \ln\left(\frac{c - c_2}{c_0 - c_2}\right)). \tag{2.21}$$

Again, theoretical results are in excellent agreement with numerical simulations for speed vs space plots (FIG. 2.5b), where all transients can be thought to be located at an initial point along the speed versus space curve. From equations (2.19 - 2.20) it is clear that stability depends on the natural time scale τ_0:

$$\tau_0 = \frac{\tau_1}{\sqrt{(1 + \frac{\tau_1}{\tau_2} - \frac{g_{syn}}{2V_t})^2 - 4\frac{\tau_1}{\tau_2}}}. \tag{2.22}$$

Based on this formula, it is easy to infer how τ_0 depends on these network constants: integration time scale(τ_1), decay time scale(τ_2), the global excitability(g_{syn}), the threshold(V_t).

If $g_{syn} \to \infty$, $\tau_0 = \mathcal{O}(g_{syn}^{-1})$, with constant slope $2V_t\tau_1$ (FIG. 2.6a). When τ_1 becomes really small, we obtain: $\lim_{\tau_1 \to 0} \tau_0 = 0$ (FIG. 2.6b). Furthermore, as the synaptic decay constant τ_2 becomes really large, we obtain $\lim_{\tau_2 \to \infty} \tau_0 = 2V_t/g_{syn} \cdot \tau_1$ (FIG. 2.6c).

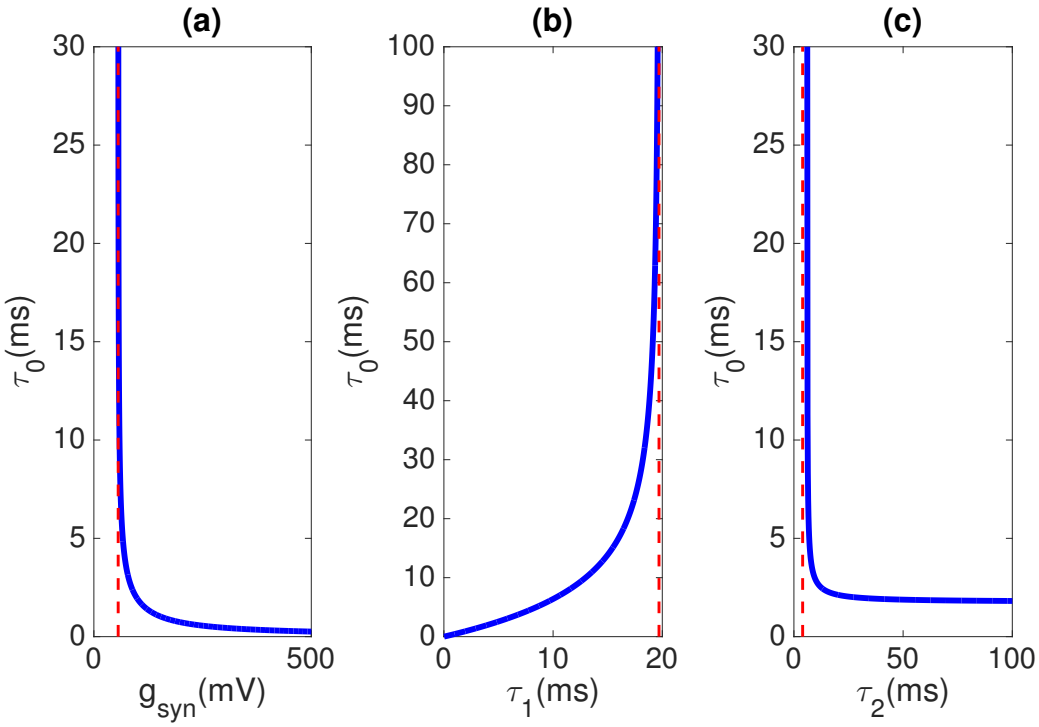

Figure (2.6) **Dependence of natural timescale τ_0 on other network parameters. (a) τ_0 vs g_{syn}.** As the excitability of the network (g_{syn}) increases, it takes less time to achieve stability (at $c = 0$ or at $c = c_2$). Here $\tau_0 = 0.12/g_{syn}$, where $g_{syn} > g_{critical} = 55.9mV$. **(b) τ_0 vs τ_1.** As the integration time τ_1 increases it takes more time to reach the stable states. When τ_1 becomes really small we obtain $\tau_0 = 0.4386\tau_1$. **(c) τ_0 vs τ_2.** Finally, when synaptic excitation lasts longer (at higher values of τ_2), stable states are also reached faster. When τ_2 becomes really large we obtain $\tau_0 = 1.7544$.

2.2.3 Reaching steady states

We now use the explicit dependence between x, t and c to determine how quickly dynamics reach the stable regimes of activity propagation, namely propagation failure at $c = 0$ or constant speed propagation at $c = c_2$. More precisely, we want to determine where the propagation stops and the amount of time it takes to achieve propagation failure. Similarly, when the initial speed is above c_1, we seek to determine the distance and time that will be needed for the propagation to reach stability, defined as reaching a value which is close to c_2,

namely $\alpha \cdot c_2$, $\alpha \approx 1$. If the initial value for propagation speed is less than c_2 we take $\alpha < 1$, otherwise we choose $\alpha > 1$. The dependence of these distances as a function of the initial speed c_0 is shown in FIG. 2.7a, while the times to reach stability are shown in Fig. 2.7b.

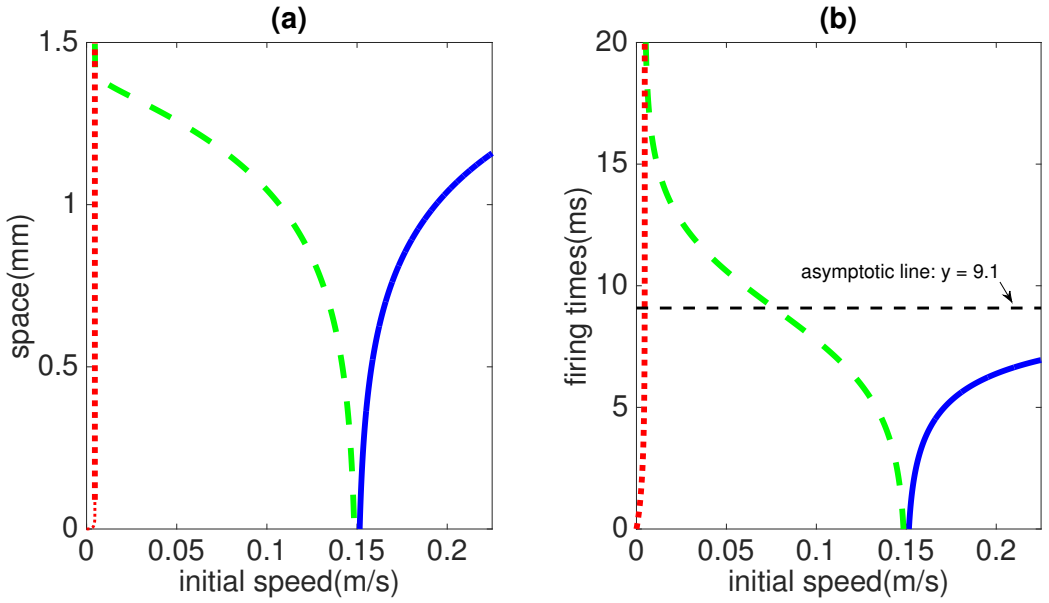

Figure (2.7) **(a) Spatial scales for achieving stable state.** We examine the distance needed to achieve stability depends on the initial speed c_0. For propagation failure this is defined as the distance traveled until speed becomes 0 (red line). For the asymptotically stable states, this is defined as the distance needed to reach $c = \alpha c_2$, where $\alpha = 0.99$ if $c_0 < c_2$ (green line) and $\alpha = 1.01$ if $c_0 > c_2$ (blue line). **(b) Temporal scales for achieving stable state.** Similar graphs are shown for the time needed to achieve stable states. In the limit where $c_0 \to \infty$ (black dotted line) stability is achieved in a finite amount of time ($t = 9.1ms$).

Using equation (2.21), we obtain the following analytical result about the amount of space needed to reach asymptotic stable state with α close to 1, due the logarithmic form which cannot take $c = c_2$,

$$x(c = \alpha c_2) = \tau_0 \cdot \ln\left(\frac{(\alpha c_2 - c_1)^{c_1}}{(\alpha c_2 - c_2)^{c_2}}\right)\left(\frac{(c_0 - c_2)^{c_2}}{(c_0 - c_1)^{c_1}}\right). \tag{2.23}$$

This reveals that when initial speed is very large, the amount of traveling space required to evolve towards stability also becomes very large, since $\lim_{c_0 \to \infty} x(c = \alpha c_2) = \infty$. Along similar lines, using equation (2.18), we can compute the amount of time needed to reach stability as follows,

$$t(c = \alpha c_2) = \tau_0 \cdot \ln(\frac{\alpha c_2 - c_1}{\alpha c_2 - c_2} \frac{c_0 - c_2}{c_0 - c_1}). \tag{2.24}$$

In contrast with the amount of space needed to reach the stable state, when c_0 is very large, only a finite time is needed in order to reach stability, since $\lim_{c_0 \to \infty} t(c = \alpha c_2) = \tau_0 \ln((\alpha c_2 - c_1)/(\alpha c_2 - c_2))$, where $\alpha > 1$.

In addition, we determine that upon reaching $c = 0$, the acceleration of the wave reaches a minimum value that does not depend on the excitability of the tissue g_{syn}, that is, $a_{min}(g_{syn}) = -\sigma/(\tau_1 \tau_2)$. We note here that this is not a global minimum, since at the other end of the spectrum, as speed becomes very large the acceleration goes to minus infinity. Finally, we note that the maximum positive acceleration, obtained at speed $(c_1 + c_2)/2$, is determined by the following equation:

$$a_{max}(g_{syn}) = \sigma((B - \frac{\tau_1 + \tau_2}{\tau_1 \tau_2})^2 - \frac{4}{\tau_1 \tau_2})/4, \tag{2.25}$$

where $B = g_{syn}/(2V_t \tau_1)$.

The dependence of a_{max} and a_{min} as a function of parameters g_{syn}, σ, τ_1 and τ_2 is shown in FIG. 2.8. Figure 2.8(a) gives the view of maximum and minimum acceleration change with the increase of global excitability g_{syn}. It is interesting to know that maximum acceleration increases with the increase of g_{syn}, while the minimum acceleration decreases to 0 when the propagation failure does not depend on g_{syn}. As what we have for speed related σ, acceleration is also linear with σ. Additionally, integration and decay time scale, maximum and minimum accelerations both go toward zero when the integration time increases. In contrast, maximum acceleration increases as the decay time scale becomes larger, and the minimum acceleration becomes zero .

All in all, we have explored the neural wave propagation with our specific type of

integrate-and-fire neural network, regarding to its speed and acceleration analytically and numerically. Acceleration is in a quadratic form of speed. With this analytical result, we dig further to understand how the network parameters relate to the propagation speed and acceleration, the dynamics that the traveling wave reaches stability or getting propagation failure, how much space and how much time needed to reach propagation stability. The mathematical expressions for the traveling wave propagation speed, space and time allow us to check the dynamics of traveling wave propagation easily and quickly.

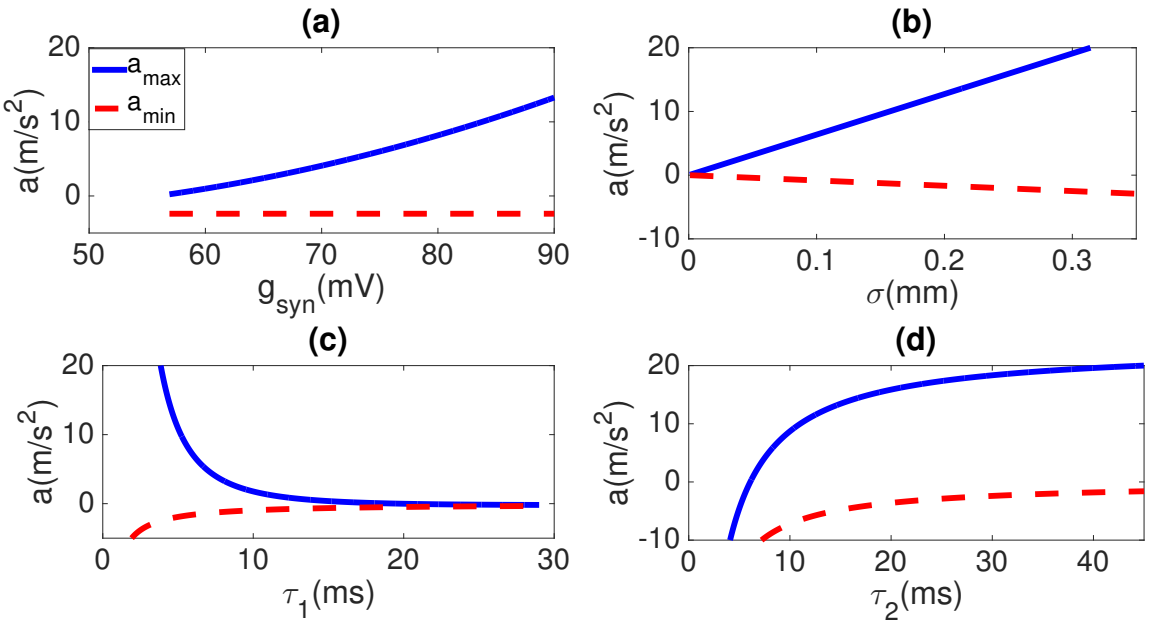

Figure (2.8) **Dependence traveling-wave acceleration on parameters. (a) acceleration vs g_{syn}.** The maximum value for acceleration (blue line) increases with excitability, while surprisingly the minimum value (red line, achieved when $c = 0$, when propagation fails) does not depend on g_{syn}. **(b) acceleration vs synaptic footprint σ.** Both maximum and minimum acceleration are linear in σ. **(c) acceleration vs integration time τ_1.** As the neural integration time becomes very large, both maximum and minimum acceleration decay toward zero values. **(d) acceleration vs decay of excitability parameter τ_2.** In contrast, only the minimum acceleration decays to zero as τ_2 becomes large, as maximum acceleration saturates to a non-zero fixed value.

2.3 Application: propagation changes in the presence of a connectivity gap

In reality, we may face a connectivity gap(non-excitable) which would decreases the traveling wave propagating speed and to some extent causes propagation failure. The research questions are how the non-excitable gap affects the traveling wave propagation and what is the minimum gap length inducing propagation failure via our mathematical neural network model and related analytical solutions explained in our previous sections.

We consider now a small section of non-excitable gap region that can be thought to be the result of local dead tissue. We are interested to determine the conditions that lead to activity propagation failure for a wave with an instantaneous speed $c > c_1$ that at $t = t_0$ reaches a non-excitable gap of length L located at position x_0. Here our new parameters for the non-excitable gap is the length of gap L and the location(x_0) where the gap starts.

To remind of what we have for the integrate-and-fire neuron at position (x) and how the voltage changes over time(t).

$$V(x,t) = \frac{g_{syn}}{2\sigma} \int_{-infty}^{x} e^{-\frac{x-y}{\sigma}} A(t - t(y))dy.$$

The neuron voltage reaches at $V(x,t) = V_t$ when it spikes, when $t = t^*(x)$ is called the firing time.

Due to the choice of the exponential kernel for the spatial synaptic connectivity function (denoted by $J(x,y)$, the voltage of the first neuron past the non-excitable gap, located at $x_1 = x_0 + L$ since x_0 is where the gap starts and L is the total length of the gap, is as following,

$$V(x_0 + L, t) = \frac{g_{syn}}{2\sigma} \int_{-\infty}^{x_0} e^{-\frac{L}{\sigma}} e^{-\frac{x_0-y}{\sigma}} A(t - t(y))dy \tag{2.26}$$

At $t = t_0$ when the neuron at position $x = x_0$ spikes, the voltage reaches V_t, we have

$$V(x_0, t_0) = V_t = J \otimes A = J \otimes A_2 - J \otimes A_1 = K_2 - K_1.$$

By what mathematical derivations that we have used in the section 2.2, we have used K_1

and K_2, where

$$K_1 = J \otimes A_1.$$

$$K_2 = J \otimes A_2.$$

$$A_1(t) = \frac{e^{-\frac{t}{\tau_1}}}{1 - \frac{\tau_1}{\tau_2}}.$$

$$A_2(t) = \frac{e^{-\frac{t}{\tau_2}}}{1 - \frac{\tau_1}{\tau_2}}.$$

Thus, we can have the following expression from equation (2.26):

$$V(x_0 + L, t_0) = g_{syn}(K_2 - K_1)e^{-\frac{L}{\sigma}} = V_T e^{-\frac{L}{\sigma}} \tag{2.27}$$

where the variables K_1 and K_2 depend on the pre-gap speed (c) as defined in equations (2.7-2.8), and they are linear of the pre-gap speed (c).

Without voltage integration during the gap, the time dependence of the voltage of neuron at position $x_1 = X_0 + L$ becomes:

$$V(x_1, t) = g_{syn}(K_2 e^{-\frac{t-t_0}{\tau_2}} - K_1 e^{-\frac{t-t_0}{\tau_1}})e^{-\frac{L}{\sigma}} \tag{2.28}$$

Depending on the speed before the gap, we have the evolution equation for the first neuron past the gap.

Due to the non-excitable gap, the neuron at position x_1 needs an additional time interval $\Delta t = \Delta t(L)$ in order to integrate the excitable current received so far and reach the threshold V_t:

$$V(x_0 + L, t_0 + \Delta t) = g_{syn}(K_2 e^{-\frac{\Delta t}{\tau_2}} - K_1 e^{-\frac{\Delta t}{\tau_1}})e^{-\frac{L}{\sigma}} = V_T \tag{2.29}$$

In general, equation (2.29) does not have an analytical solution for the extra time for the neuron at $x_1 = x_0 + L$ to spike with fixed gap length L, but we can the expression of pre-gap speed regarding to Δt and L,

$$c = \frac{V_t e^{L/\sigma}/g_{syn} - (b_1 e^{-\Delta_t/\tau_2} - b_2 e^{-\Delta_t/\tau_1})}{a_1 e^{-\Delta_t/\tau_2} - a_2 e^{-\Delta_t/\tau_1}}. \tag{2.30}$$

where

$$K_1 = a_1 c + b_1.$$

$$K_2 = a_2 c + b_2.$$

where a_1, a_2, b_1, b_2 are constant values related with V_t, g_{syn},τ_1 and τ_2.

$$a_1 = \frac{V_t}{g_{syn}\sigma}(\frac{1}{\tau_1} - \frac{1}{\tau_2}).$$

$$a_2 = \frac{V_t}{g_{syn}\sigma}(\frac{1}{\tau_1} - \frac{1}{\tau_2}).$$

$$b_1 = \frac{V_t}{g_{syn}\tau_2}(\frac{1}{\tau_1} - \frac{1}{\tau_2}).$$

$$b_2 = \frac{V_t}{g_{syn}\tau_1}(\frac{1}{\tau_1} - \frac{1}{\tau_2}).$$

Following the procedure outlined in equations (2.7 - 2.8), we obtain the first order equation in the speed of propagation after passing the gap, c_{gap}:

$$K_2\big(\frac{1}{\sigma} + \frac{1}{c_{gap}\tau_2}\big)e^{-\frac{\Delta t}{\tau_2}} = K_1\big(\frac{1}{\sigma} + \frac{1}{c_{gap}\tau_1}\big)e^{-\frac{\Delta t}{\tau_1}} \tag{2.31}$$

The solution for $c_{gap} = c_{gap}(c, L)$ then becomes:

$$c_{gap}(c, L) = \sigma \frac{\frac{K_1(c)}{\tau_1} e^{-\frac{\Delta t(L)}{\tau_1}} - \frac{K_2(c)}{\tau_2} e^{-\frac{\Delta t(L)}{\tau_2}}}{K_2(c) e^{-\frac{\Delta t(L)}{\tau_2}} - K_1(c) e^{-\frac{\Delta t(L)}{\tau_1}}} \tag{2.32}$$

The failure condition after passing the gap is simply $c_{gap}(c, L) < c_1$. Numerical result for this condition is illustrated, for fixed c in Fig.2.9a, different colored lines denote different pre-gap speed, they are, $c = 0.0386, c = 0.0773, c = 0.15, c = 0.3$. Also for fixed L in Fig.2.9b, we plot the after-gap speed versus the pre-gap speed with different fixed L from $0.05mm$ to $0.35mm$. We can see that the rate of speed change is getting larger and larger with longer non-excitable gap.

In addition, we compute the minimum amount of non-excitable gap length that would prevent any further propagation of activity for waves that reach the gap with speed c, as shown in FIG.2.9c.

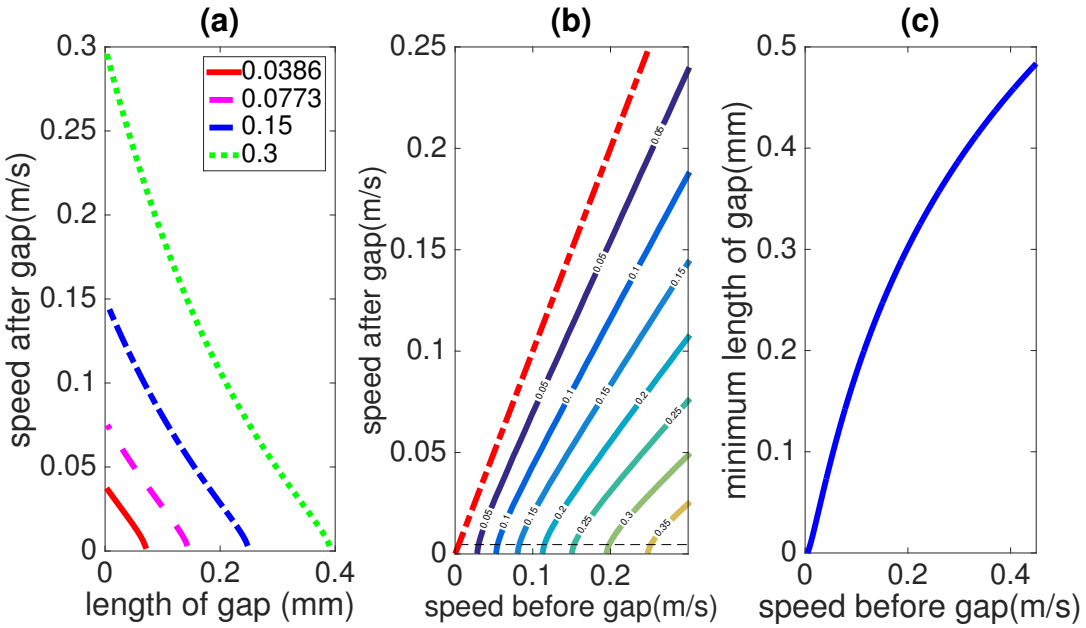

Figure (2.9) **Activity propagation changes induced by a non-excitable region of length L. (a) Speed after gap vs length of gap.** Not surprisingly, larger non-excitable regions decrease the speed of the traveling waves past the gap and they could even lead to propagation failure at $c = 0$. We plot this relationship for four initial conditions: $c = 0.0386$, $c = 0.0773$, $c = 0.15$ and $c = 0.3$. **(b) Speed after gap vs speed before gap.** Slow traveling waves are more affected by a constant length gap and may even fail, while fast ones only show a moderate loss in speed as they propagate further away. The red dotted line is the $y = x$, corresponding to zero speed loss and it is included here for comparison with the other contour lines. Obviously, with the increase of gap length, the change rate of speed before and after gap increases. Length of the gaps considered here range from $L = 0.05$ mm to $L = 0.35$ mm, with eight uniformly spaced values considered here. **(c) Minimum length of gap that causes propagation failure as a function of the speed before gap.** We determine that propagation eventually fails when speed becomes less than c_1. Taking into account the speed before gap, the graph determines the minimum length of gap needed to reach propagation failure.

The result is quite interesting when we face a short dead tissue which is not excitable.

From our model, we can determine the minimum length of gap inducing propagation failure given pre-gap speed, which mean we can also determine the Δ_t for the first neuron after the gap to spike, as well as the after-gap speed. We have applied analytical results from the case without dead tissue to help solve the dead tissue problem quickly. Next, we will discuss about a more general case when the synaptic connectivity function is not only limited to exponential kernel.

2.4 Applications to more general connectivity functions

The analytical results obtained so far depend on the specific choice of an exponential kernel for the spatial connectivity function. However, our approach can be extended to more general classes of functions. We now consider a more complicated spatial connectivity function, a first order polynomial times the exponential function which actually can fit to any functions, which has the coefficient term to scale the connectivity function,

$$coef = \frac{a\Delta_d + b}{2\sigma(a\sigma + b)}.$$

So as to,

$$\int_D J(x,y) = 1.$$

Thus, we have the spatial synaptic connectivity function,

$$J(x,y) = \frac{a|x-y|e^{\frac{-|x-y|}{\sigma}}}{2\sigma(a\sigma+b)} + \frac{b \cdot e^{\frac{-|x-y|}{\sigma}}}{2\sigma(a\sigma+b)}. \tag{2.33}$$

Let

$$J_1 = \frac{a|x-y|e^{\frac{-|x-y|}{\sigma}}}{2\sigma(a\sigma+b)}. \tag{2.34}$$

$$J_2 = \frac{b \cdot e^{\frac{-|x-y|}{\sigma}}}{2\sigma(a\sigma + b)}. \tag{2.35}$$

Figure 2.10 illustrated the difference between the homogeneous exponential coupling function and the one that we have modified by multiplying a polynomial function. The one that we have modified with polynomial function becomes less compact compared with the exponential coupling.

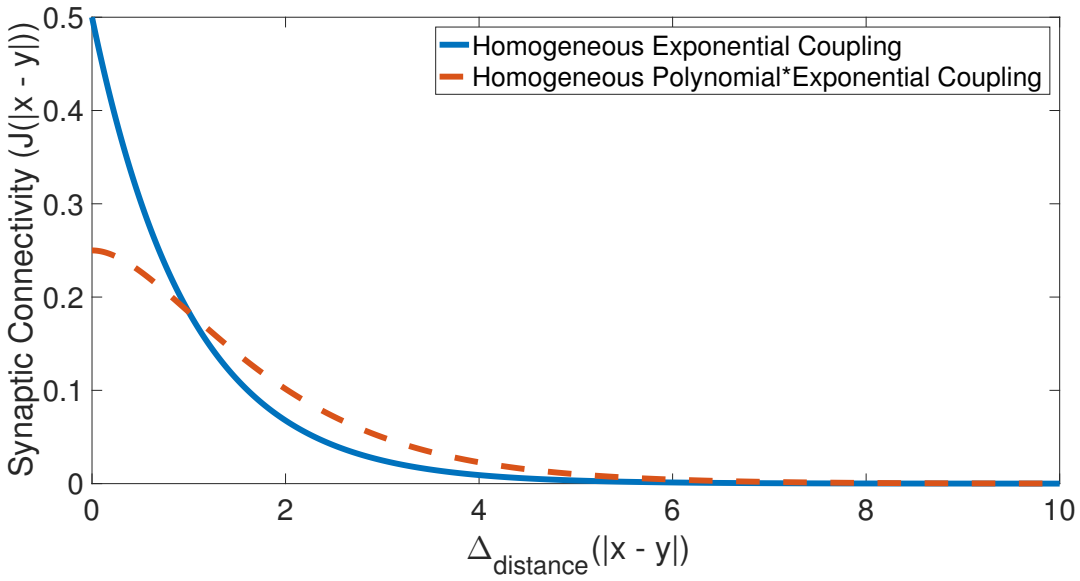

Figure (2.10) **Synaptic coupling functions.** More general coupling function(2.33)(red curve) is applied to the system with parameters $a = 1, b = 1$. Compared with the exponential coupling function(blue curve), the new modified coupling function has wider synaptic connectivity of the distance between neurons. Within small distances, the exponential coupling function gives stronger synaptic connectivity. $\sigma = 1$ is used here for showing not too small numbers in axises.

A consistency equation for a traveling wave that comes from $-\infty$ with speed c can be obtained by using $t^*(x) = x/c$. Without loss of generality, at $t = 0$ the wave will pass

through $x = 0$. Therefore, we obtain

$$V(x = 0, t = 0) = V_T.$$

and we obtain our new evolution equation for traveling wave spiking times along the neural slice.

$$V_T = g_{syn} \int_{-\infty}^{0} \frac{a|y| + b}{2\sigma(a\sigma + b)} e^{\frac{-|y|}{\sigma}} \cdot \frac{e^{\frac{-|t(y)|}{\tau_2}} - e^{\frac{-|t(y)|}{\tau_1}}}{1 - \frac{\tau_1}{\tau_2}} dy$$

With substitution

$$t^*(y) = y/c.$$

Neuron at position y has the traveling wave speed equals c, when it spikes at $t = t^*(y)$. We obtain the evolution equation V_T is a function of the location y and traveling wave speed (c).

$$V_T = g_{syn} \int_{-\infty}^{0} \frac{a|y| + b}{2\sigma(a\sigma + b)} e^{\frac{-|y|}{\sigma}} \cdot \frac{e^{\frac{-|y|}{c\tau_2}} - e^{\frac{-|y|}{c\tau_1}}}{1 - \frac{\tau_1}{\tau_2}} dy \tag{2.36}$$

We can then express the membrane voltage as a function of traveling wave speed through integration by parts,

$$\begin{aligned} V_T = \quad & B \int_{-\infty}^{0} a|y|(e^{1/c}(e^{-|y|/(\sigma+\tau_2)} + e^{-|y|/(\sigma+\tau_1)})) + \\ & B \int_{-\infty}^{0} b(e^{1/c}(e^{-|y|/(\sigma+\tau_2)} + e^{-|y|/(\sigma+\tau_1)})) \end{aligned}$$

where B is a constant related with parameters: $g_{syn}, \sigma, a, b, \tau_1, \tau_2$,

$$B = \frac{g_{syn}}{2\sigma(a\sigma + b)(1 - \frac{\tau_1}{\tau_2})}.$$

As a result, the membrane voltage has the following form as a function of traveling wave

speed, with parameters a and b are the weights of synaptic connectivity function.

$$V(c) = \frac{g_{syn}}{2\sigma(a\sigma+b)(1-\frac{\tau_1}{\tau_2})}\Big[\frac{a\sigma}{(\frac{1}{\sigma}+\frac{1}{c\tau_2})^2} - \frac{a\sigma}{(\frac{1}{\sigma}+\frac{1}{c\tau_1})^2} + \frac{b}{\frac{1}{\sigma}+\frac{1}{c\tau_2}} - \frac{b}{\frac{1}{\sigma}+\frac{1}{c\tau_1}}\Big] \tag{2.37}$$

We choose similar parameters to the exponential case in order to obtain a stable traveling wave with exact same fast-stable speed (Fig. 2.11), such that $a = 1, b = 1$. The other parameters are the same as before. From figure 2.11, we can find two interaction points with $V_t = 150mV$, which are our two speed solutions as we've found.

It is easy to see when speed goes to either zero or ∞ the membrane potential $V(c)$ becomes zero. This guarantees that for large enough global network excitability g_{syn} there will be at least traveling waves solutions. Therefore, we will proceed to check if we can general speed solution from this more complicated neural model network.

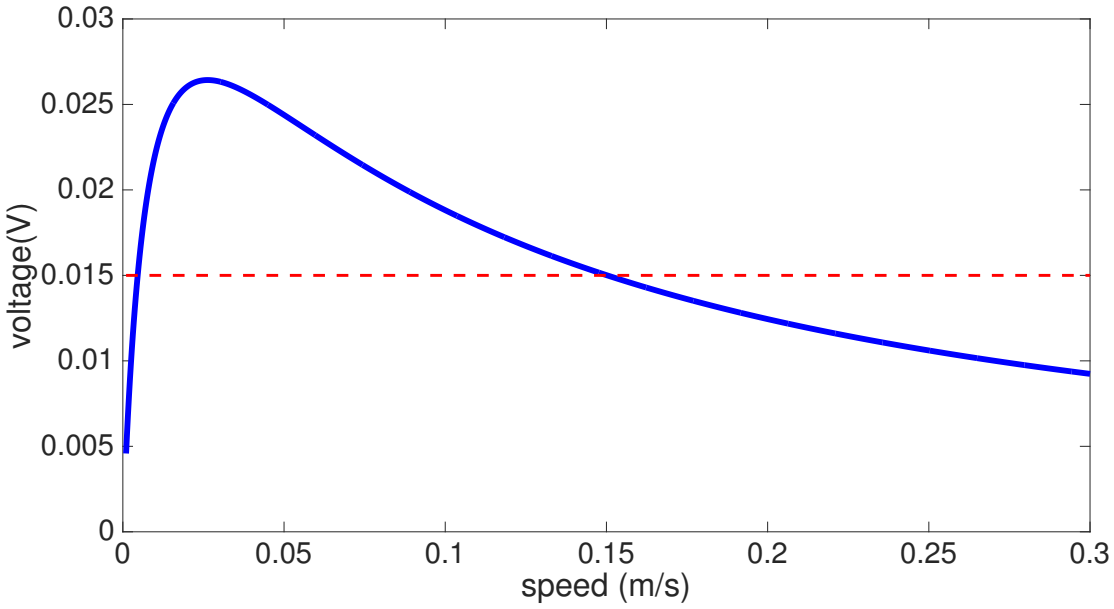

Figure (2.11) **Voltage changes over speed by applying polynomial coupling function** More general coupling function(2.33) is applied to the system with parameters $a = 1, b = 1, \tau_1 = 4 \times 10^{-3}s, \tau_2 = 3.0 \times 10^{-2}s, \sigma = 2.88 \times 10^{-4}m, g_{syn} = 9.85 \times 10^{-2}V, Vt = 1.5 \times 10^{-2}V$. Two speed solutions exist when voltage reaches threshold ($V_T = 1.5 \times 10^{-2}V$).

Equation $V(c) = V_t$ can be written as a fourth order polynomial equation, as we have derived a second order polynomial equation from the neural network with exponential kernel synaptic connectivity.

We now follow the same procedure for the exponential case, namely generate enough derivatives of the original equation in order to solve all convolution terms as function of the time derivatives t', t'' and higher order terms. We use these terms in order to obtain an equation that contains only these derivative, that is in general,

$$t^{(n)} = f(t', t'', ..., t^{(n-1)}). \tag{2.38}$$

Because the system of three equations (2.4-2.6) contains 4 unknowns, because we have

J_1 and J_2, and each of them has two unknowns, $J_i \otimes A_j$ ($\{i,j\} \in \{1,2\}$). Besides, only computation of an extra derivative is needed which is the fourth order derivative, since due to the specific form of the connectivity kernel no new kind of functions will been created as a result of taking the derivatives of the spatial function J.

Those unknowns can be computed as function of t', t'' and t''' using three equations (2.4-2.6), along with the third order derivative of equation (2.4):

$$\begin{aligned}(J \otimes A)''' = J''' \otimes A + 3t' J'' \otimes A' + 3(t')^2 J' \otimes A'' + \\ t''' J \otimes A' + (t')^3 J \otimes A''' + 3t'' J' \otimes A' + t' t'' J \otimes A'' \\ + 2t' J_0' A_0' + 2t'' J_0 A_0' + (t')^2 J_0 A_0'' = 0 \quad (2.39)\end{aligned}$$

Taking one more derivative, namely the derivative of equation (2.39), will connect 4^{th} order derivative with the lower order derivatives of t, thus generating an ordinary differential equation, similar to the case analyzed earlier:

$$\begin{aligned}J'''' \otimes A + 4(t')^3 J' \otimes A''' + 4t''' J' \otimes A' + 4t' J''' \otimes A' + \\ 6t'' J'' \otimes A' + 6(t')^2 J'' \otimes A'' + 3(t'')^2 J \otimes A'' + (t')^4 \\ J \otimes A'''' + \mathbf{t}'''' \cdot J \otimes A' + 4t' t''' J \otimes A'' + 6(t')^2 t'' J \otimes A''' \\ + 12t' t'' J' \otimes A'' + 5t'' J_0' A_0' + 2t''' J_0 A_0' + 3t' t'' J_0 A_0'' + \\ 3t' J_0'' A_0' + 3(t')^2 J_0' A_0'' + (t')^3 J_0 A_0''' + t' t'' J_0 A_0' = 0 \quad (2.40)\end{aligned}$$

We verified that network dynamics are in agreement with this ODE system, using numerical simulations to compute values for the first three derivatives of t as initial conditions and making use of the explicit solution $t'''' = f(t', t'', t''')$ from equation (2.40), as illustrated in FIG. 2.12.

Although the transition toward constant speed waves is now much more complicated

and analytical solutions do not likely exist for this case, again local dynamics determine the evolution of the wave. More precisely, two waves that have the same values for the first three derivatives of t at a spatial location x_0 will follow identical trajectories for $x > x_0$.

This approach works for any synaptic connectivity function J who is a product of a polynomial in x and the exponential function, since no new functions will be generated through higher order derivatives of function J. Here, the number of equations needed to transform the evolution equation into an ODE is,

$$N = 2n + 3,$$

where n is the degree of the polynomial, with $2n + 2$ derivatives of original equation (2.4) needed.

In fact this approach works for any function J that generates a finite set of functions through the process of taking derivatives. For example, combinations of polynomials, sine and cosine functions times the exponential, would also generate a finite set of functions through derivative steps. One function that cannot be used is the gaussian function

$$J(x) = e^{(-x^2/(2\sigma^2))}/\sqrt{2\pi\sigma},$$

since at each step of the procedure the computation of higher order derivatives keeps generating new functions such as

$$xe^{-x^2/(2\sigma^2)},$$
$$x^2e^{-x^2/(2\sigma^2)},$$

and higher order polynomials times the original gaussian function.

As a result, it is not possible to solve and express the convolution unknowns as func-

tions of derivatives of t. Nevertheless, the more advantageous property of continuous first order derivative that the gaussian function has over the exponential kernel, can be offset by properly chosen set of functions such as $(1 + |x|)e^{-|x|}$.

Therefore, somehow surprisingly, activity propagation depends on local quantities only for longer range kernels such as products of polynomial and exponential functions, but not for gaussian and other similar, more localized, types of functions. In effect, the more localized kernels ensure that the local details of the firing map are important for further propagation, while the longer range kernels analyzed here ensure that a neighborhood of neurons close to firing are less susceptible of the details of the excitation that brought them close to the threshold.

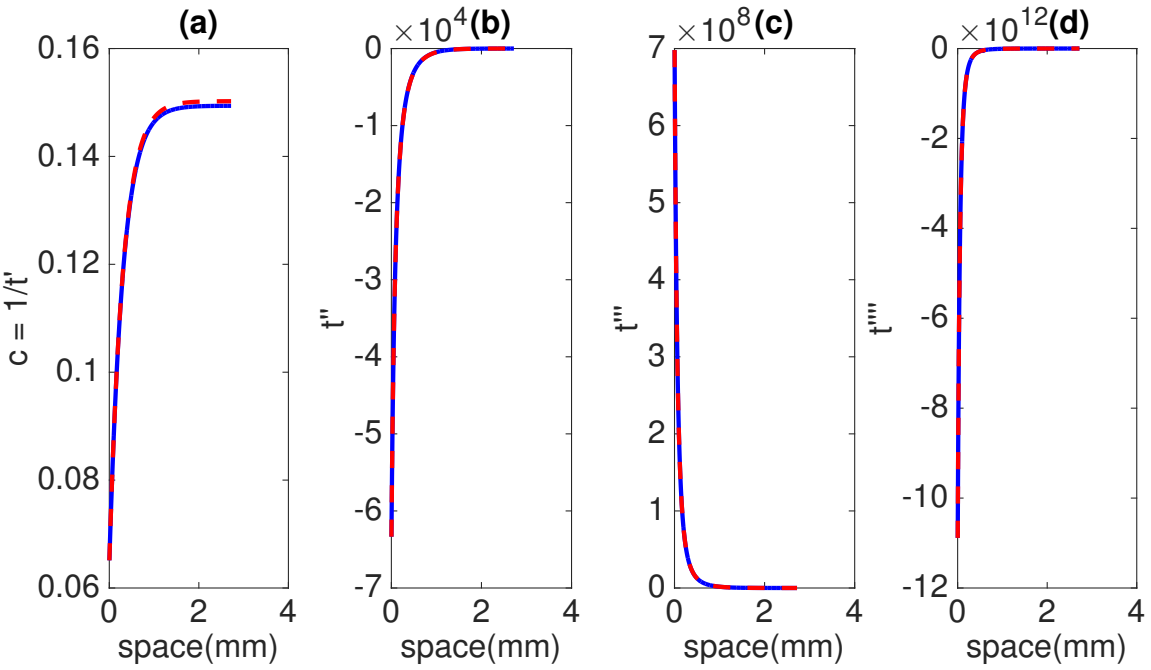

Figure (2.12) **Successive derivatives of firing times.** Numerical simulations (blue) are in excellent agreement with the the dynamics of ODE system, as illustrated by the first four derivatives of firing map (equations 2.4-2.6, 2.39-2.40, red lines): **(a)** t', **(b)** t'', **(c)** t''' and **(d)** t''''. Similar to the previous cases considered, an initial region is induced to spike to the left of $x > 0$ region in order to provide the initial activity propagation. This is used to extract the initial conditions for the ODE system, such as the initial speed, $1/t'(0)$ as well as the next two derivatives, $t''(0)$ and $t'''(0)$.

2.5 Neural network extended to multiple spiking neurons

The previous integrate-and-fire neural networks are all based on the assumption that the integrate-and-fire neurons only spikes once. As our major simplification, you may ask if our model can extend to multiple spiking neural network. The answer is positive. We can easily extend our mathematical model into the multiple spiking case.

We can write the integral form of integrate-and-fire model with single spike as follows,

$$V_1(x,t) = \frac{g_{syn}}{1-\frac{\tau_1}{\tau_2}} \int_{-\infty}^{x} \frac{e^{-\frac{x-y}{\sigma}}}{2\sigma} (e^{-\frac{t-t_1^*(y)}{\tau_2}} - e^{-\frac{t-t_1^*(y)}{\tau_1}}) dy, \tag{2.41}$$

where $t_1^*(y)$ is the single spiking time for the neuron at location y, which the same one as we've used.

When the neurons can spike multiple times, the integral form of the first wave front is

$$V_1(x,t) = \frac{g_{syn}}{1-\frac{\tau_1}{\tau_2}} \sum_{k=1}^{\infty} \int_{-\infty}^{x-\eta_{1,k}(x)} \frac{e^{-\frac{x-y}{\sigma}}}{2\sigma} (e^{-\frac{t-t_k^*(y)}{\tau_2}} - e^{-\frac{t-t_k^*(y)}{\tau_1}}) dy, \tag{2.42}$$

where $t_k^*(y)$ is the k_{th} spiking time for the neuron at location y. $\eta_{1,k}(x)$ is the gap from k_{th} spiking wave.

At the spiking moment, $V_1(x,t) = V_T$, yielding

$$V_T = \frac{g_{syn}}{1-\frac{\tau_1}{\tau_2}} \sum_{k=1}^{\infty} \int_{-\infty}^{x-\eta_{1,k}(x)} \frac{e^{-\frac{x-y}{\sigma}}}{2\sigma} (e^{-\frac{t^*(x)-t_k^*(y)}{\tau_2}} - e^{-\frac{t^*(x)-t_k^*(y)}{\tau_1}}) dy. \tag{2.43}$$

In the following derivations, t is used as spiking time for simplification. Let

$$\begin{aligned} P(x) &= e^{-x/\sigma}, \\ \alpha_i(x) &= e^{-t/\tau_i}, \\ Q_i(x) &= \sum_{k=1}^{\infty} \int_{-\infty}^{x-\eta_{1,k}(x)} e^{y/\sigma} e^{t_k(y)/\tau_i}, i = 1, 2. \end{aligned}$$

Then, the evolution equation of spiking neurons becomes

$$\frac{V_T}{g} 2\sigma(1-\frac{\tau_1}{\tau_2}) = P(x)\alpha_2(x)Q_2(x) - P(x)\alpha_1(x)Q_1(x). \tag{2.44}$$

Taking the first derivative with respect to x,

$$0 = (P(x)\alpha_2(x)Q_2(x) - P(x)\alpha_1(x)Q_1(x))'.$$

Since,

$$\begin{aligned}
Q_i'(x) =&(\sum_{k=1}^{\infty}\int_{-\infty}^{x-\eta_{1,k}(x)} e^{y/\sigma}e^{t_k(y)/\tau_i})'\\
=&\sum_{k=1}^{\infty} e^{\frac{x-\eta_{1,k}(x)}{\sigma}}e^{\frac{t_k(x-\eta_{1,k}(x))}{\tau_i}}(1-\eta_{1,k}'(x))\\
=&\sum_{k=1}^{\infty} e^{\frac{x-\eta_{1,k}(x)}{\sigma}}e^{\frac{t_1(x)}{\tau_i}}(1-\eta_{1,k}'(x))\\
=&e^{\frac{x}{\sigma}}e^{\frac{t_1(x)}{\tau_i}}\sum_{k=1}^{\infty} e^{\frac{-\eta_{1,k}(x)}{\sigma}}(1-\eta_{1,k}'(x))\\
=&e^{\frac{x}{\sigma}}e^{\frac{t_1(x)}{\tau_i}}\sum_{k=1}^{\infty} e^{\frac{-\eta_{1,k}(x)}{\sigma}}(\frac{t_k'(x-\eta_{1,k}(x))}{t_1'(x)}).
\end{aligned}$$

In any case,

$$P(x)\alpha_2(x)Q_2'(x) - P(x)\alpha_1(x)Q_1'(x) = 0$$

Thus the first derivative equals,

$$0 = -P\alpha_2Q_2(\frac{1}{\sigma}+\frac{t_1'(x)}{\tau_2}) + P\alpha_1Q_1(\frac{1}{\sigma}+\frac{t_1'(x)}{\tau_1}). \tag{2.45}$$

Now take the second derivative:

$$\begin{aligned}
0 =&(-P\alpha_2Q_2(\frac{1}{\sigma}+\frac{t_1'(x)}{\tau_2}) + P\alpha_1Q_1(\frac{1}{\sigma}+\frac{t_1'(x)}{\tau_1}))'\\
0 =&P\alpha_2Q_2((\frac{1}{\sigma}+\frac{t_1'(x)}{\tau_2})^2 - \frac{t_1''(x)}{\tau_2})-\\
&P\alpha_1Q_1((\frac{1}{\sigma}+\frac{t_1'(x)}{\tau_1})^2 - \frac{t_1''(x)}{\tau_1}) - (\frac{1}{\sigma}+\frac{t_1'(x)}{\tau_2})P\alpha_2Q_2' + (\frac{1}{\sigma}+\frac{t_1'(x)}{\tau_1}))P\alpha_1Q_1'.
\end{aligned}$$

Let

$$\begin{aligned}
Z(x) =&\sum_{k=1}^{\infty} e^{\frac{-\eta_{1,k}(x)}{\sigma}}(\frac{t_k'(x-\eta_{1,k}(x))}{t_1'(x)})\\
=&\sum_{k=1}^{\infty} e^{\frac{-\eta_{1,k}(x)}{\sigma}}\frac{c_1(x)}{c_k(x-\eta_{1,k}(x))}.
\end{aligned}$$

Thus the second derivative equals,

$$\begin{aligned} 0 =& P\alpha_2 Q_2((\frac{1}{\sigma}+\frac{t_1'(x)}{\tau_2})^2-\frac{t_1''(x)}{\tau_2})- \\ & P\alpha_1 Q_1((\frac{1}{\sigma}+\frac{t_1'(x)}{\tau_1})^2-\frac{t_1''(x)}{\tau_1})+(\frac{1}{c_1(x)\tau_1}-\frac{1}{c_1(x)\tau_2})Z(x). \end{aligned} \tag{2.46}$$

By Eq.(3.4) and Eq.(3.5), we can solve for $P\alpha_1 Q_1$ and $P\alpha_2 Q_2$, which are the same as the single spike case(K_1 and K_2),

$$\begin{aligned} P\alpha_1 Q_1 =& \frac{V_T}{g} 2\sigma(1-\frac{\tau_1}{\tau_2})\frac{\frac{1}{\sigma}+\frac{1}{c\tau_2}}{\frac{1}{c}(\frac{1}{\tau_1}-\frac{1}{\tau_2})} \\ P\alpha_2 Q_2 =& \frac{V_T}{g} 2\sigma(1-\frac{\tau_1}{\tau_2})\frac{\frac{1}{\sigma}+\frac{1}{c\tau_1}}{\frac{1}{c}(\frac{1}{\tau_1}-\frac{1}{\tau_2})} \end{aligned}$$

Then we can rewrite Eq.(3.6) into $a_1(x)$ of $c_1(x)$, first wave front's acceleration of speed by the relation,

$$\frac{d^2t}{dx^2} = -\frac{a}{c^3},$$

$$a_1(x) = -\frac{(c_1(x)+\frac{1}{\tau_1})(c_1(x)+\frac{\sigma}{\tau_2})}{\sigma} + \frac{g c_1(x) Z(x)}{2V_T\tau_1}, \tag{2.47}$$

where

$Z(x) = 1$ in the single spiking network in homogeneity;

$Z(x) = \sum_{k=1}^{\infty} e^{\frac{-\eta_{1,k}(x)}{\sigma}} \frac{c_1(x)}{c_k(x-\eta_{1,k}(x))}$ in the multiple spiking network in homogeneity;

CHAPTER 3

ACTIVITIES OF TRAVELING WAVE PROPAGATION IN PERIODIC INHOMOGENEITIES

3.1 Evolution equations with inhomogeneities

In reality, neurons face periodic inhomogeneities when there is shift in phase and amplitude change. This is what we are going to study that in this section. The methods that we have used in homogeneous integrate-and-fire neuron network can also be adapted to the case of a heterogeneous medium. In this section, we applied two periodic inhomogeneity modulations to our network: a constant periodic change and a cosine function, characterized by periodic length and amplitude. Critical speeds could be obtained from our model and we could provide a precise explanation of when the wave speed are increasing, decreasing or will stop eventually regarding to different network parameters and neuron parameters. In the cosine form of inhomogeneity, exact speed solution is difficult to obtain since it becomes more complicated with changing inhomogeneity values by locations. Furthermore, we looked at the approximations of speed numerically.

As we have used in our homogeneous integrate-and-fire neural network, we will extend the integrate-and-fire neural network with the same single spike assumption and the firing time is a monotonic function of their position x, that is, $t_x^* > t_y^*$ if $x > y$. Please go back to last section to find out why.

$$V(x,t) = g_{syn} \int_{-\infty}^{x} J(x,y) A(t - t_y^*) dy, \tag{3.1}$$

where g_{syn} is the global excitability of the network, t_y^* denotes the firing time for the neuron at position y. $J(x,y)$ describes the spatial connectivity between neurons at positions x and y. $A(t)$ describes the excitation provided by a presynaptic spike onto the postsynaptic

neuron at position x. The functions $J(x,y)$ and $A(t)$ take in the following explicit form, which is different from the homogeneous model, the synaptic function is multiplied by a inhomogeneous term($K(y)$),

$$J(x,y) = \frac{e^{-|x-y|/\sigma}}{2\sigma}(1+K(y)), \tag{3.2}$$

$$A(t) = \frac{e^{-t/\tau_2} - e^{-t/\tau_1}}{1-\tau_1/\tau_2}, \tag{3.3}$$

where τ_1 is the integration time constant of the membrane, τ_2 the time constant for the decay of the synaptic excitation where $\tau_2 > \tau_1$, σ is the spatial constant for the neuronal interaction. $K(y)$ is the kernel function that adds inhomogeneity to the neurons' synaptic connectivity.

In order to figure out the firing times in the integral form and characterize the dynamics of propagation of activities (t is used as spiking time at position x in the following expressions), we examine the speed ($c(x) = dx/dt = 1/t'$) and acceleration ($a(x) = d^2x/dt^2 = -c^3t''$) from the derivatives of firing times by the following transformation,

$$\begin{aligned} a(x) = \frac{d^2x}{dt_x^2} &= \frac{dx}{dt_x}\left(\frac{1}{\frac{dt_x}{dx}}\right) = -\frac{1}{(\frac{dt_x}{dx})^2}\frac{d^2t_x}{x^2}\frac{dx}{dt_x} \\ &= -c^3\frac{d^2t_x}{dx^2} = -c^3t''. \end{aligned}$$

Since neurons are exponentially coupled, the derivatives do not generate extra terms in x from derivatives as we've used in the multiple spike neurons evolution equation derivation,

let

$$
\begin{aligned}
P(x) &= e^{-x/\sigma}, \\
\alpha_i(x) &= e^{-t/\tau_i}, \\
Q_i(x) &= \int_{-\infty}^{x} e^{y/\sigma} e^{t^*(y)/\tau_i} K(y) dy, \\
i &= 1, 2.
\end{aligned}
$$

Thus, Eq. 3.1 becomes

$$
\frac{2\sigma(1-\frac{\tau_1}{\tau_2})V_T}{g_{syn}} = (P\alpha_2 Q_2 - P\alpha_1 Q_1)(x). \tag{3.4}
$$

The first derivative of Eq. 3.1 or Eq. 3.4 with respect to x is

$$
0 = -P\alpha_2 Q_2(\frac{1}{\sigma} + \frac{t'(x)}{\tau_2}) + P\alpha_1 Q_1(\frac{1}{\sigma} + \frac{t'(x)}{\tau_1}), \tag{3.5}
$$

since,

$$
\begin{aligned}
Q_i'(x) &= (\int_{-\infty}^{x} e^{y/\sigma} e^{t_y^*)/\tau_i} K(y) dy)' = e^{\frac{x}{\sigma}} e^{\frac{t}{\tau_i}} K(x), \\
P(x)\alpha_i(x) Q_i'(x) &= K(x).
\end{aligned}
$$

By Eq.(3.4) and Eq.(3.5), we can solve for $P\alpha_1 Q_1$ and $P\alpha_2 Q_2$, which are the same as in the homogeneous network,

$$
\begin{aligned}
P\alpha_1 Q_1 =& \frac{V_T}{g_{syn}} 2\sigma(1-\frac{\tau_1}{\tau_2}) \frac{\frac{1}{\sigma} + \frac{1}{c\tau_2}}{\frac{1}{c}(\frac{1}{\tau_1} - \frac{1}{\tau_2})}, \\
P\alpha_2 Q_2 =& \frac{V_T}{g_{syn}} 2\sigma(1-\frac{\tau_1}{\tau_2}) \frac{\frac{1}{\sigma} + \frac{1}{c\tau_1}}{\frac{1}{c}(\frac{1}{\tau_1} - \frac{1}{\tau_2})}.
\end{aligned}
$$

Then we take the second derivative of Eq. 3.4 and obtain the following equation con-

taining t' and t'',

$$\begin{aligned} 0 =& P\alpha_2 Q_2((\frac{1}{\sigma}+\frac{t'}{\tau_2})^2-\frac{t''}{\tau_2}) \\ & - P\alpha_1 Q_1((\frac{1}{\sigma}+\frac{t'}{\tau_1})^2-\frac{t''}{\tau_1})+K(x)(\frac{t'}{\tau_1}-\frac{t'}{\tau_2}). \end{aligned} \tag{3.6}$$

By the results of $P\alpha_1 Q_1$ and $P\alpha_2 Q_2$ we can write Eq.(3.6) into an equation of first wave front's acceleration as a function of speed with certain inhomogeneity,

$$a(x) = -\frac{(c(x)-c_1)(c(x)-c_2)}{\sigma} + Bc(x)K(x) \tag{3.7}$$

where c_1 and c_2, the speed for the slow-unstable and the fast-stable constant speed traveling wave solutions respectively, depend only on network parameters σ, τ_1, τ_2, V_T, g_{syn} as shown here explicitly.

$$c_{1,2} = \sigma/2\Big((B-\beta) \mp \sqrt{(B-\beta)^2-\frac{4}{\tau_1\tau_2}}\ \Big), \tag{3.8}$$

where $B = g_{syn}/(2V_t\tau_1), \beta = (\tau_1+\tau_2)/(\tau_1\tau_2)$, $K(x)$ is the inhomogeneous term which we will discuss next in different forms.

From what we have for homogeneous and non-homogeneous neural network, the analytical results for acceleration as a function of speed is not changed a lot. The only difference is that we have an extra term besides the quadratic term. The extra term relates to the inhomogeneous form with coefficient$(g_{syn}/(2V_T\tau_1))$.

3.2 Illustration of propagation failure with constant periodic inhomogeneity

In this section, we consider first a special form of inhomogeneity to our neural network, which is constantly alternating inhomogeneity (ϵ) with changing period denoted by λ. Here are the equations,

$$K(x) = \begin{cases} \epsilon, \\ -\epsilon. \end{cases}$$

or

$$K(x) = (-1)^{[x/\lambda]}\epsilon \tag{3.9}$$

Thus the ordinary differential equation for speed is

$$\sigma\frac{dc}{dx} = -\frac{(c(x)-c_1)(c(x)-c_2)}{c(x)} + \sigma B(-1)^{[x/\lambda]}\epsilon \tag{3.10}$$

Since

$$a = c\frac{dc}{dx}.$$

With this constant periodic inhomogeneity, we can obtain the analytical solution from (3.10),

$$\begin{aligned} x &= f(m,c) \\ &= \frac{(c_1+c_2+m)tan^{-1}(\frac{-c_1-c_2-m+2c}{\sqrt{-c_1^2+2c_1(c_2-m)-(c_2+m)^2}})}{\sqrt{-c_1^2+2c_1(c_2-m)-(c_2+m)^2}} \\ &+ \ln\{c_1(c_2-c)+c(-c_2-m+c)\}/2 + k_1, \end{aligned} \tag{3.11}$$

when it is positive inhomogeneity,

$$m = \sigma B.$$

and when it is negative inhomogeneity,

$$m = -\sigma B.$$

where k_1 is a constant value depending on the initial condition.

If we take integral of one period λ when $K(x) = \epsilon$, where speed changes from c_0 to c_f, where c_0 denotes the lowest speed point and c_f denotes the highest point that a period of traveling wave speed goes from c_0 to c_f and back to c_0.

$$\int_0^{\lambda} dx = \int_{c_0}^{c_f} \sigma \frac{dc}{-\frac{(c-c_1)(c-c_2)}{c} + \sigma B\epsilon},$$
$$\lambda = \int_{c_0}^{c_f} \sigma \frac{cdc}{-(c - cp_1)(c - cp_2)},$$

where

$$cp_1 = \frac{c_1 + c_2 + \sigma B\epsilon - \sqrt{(c_1 + c_2 + B\epsilon)^2 - 4c_1c_2}}{2}, \tag{3.12}$$
$$cp_2 = \frac{c_1 + c_2 + \sigma B\epsilon + \sqrt{(c_1 + c_2 + B\epsilon)^2 - 4c_1c_2}}{2}. \tag{3.13}$$

Then continued with the next period when $K(x) = -\epsilon$, where speed changes from c_f to c_0, with

$$-(c - c_1)(c - c_2) - c\sigma B\epsilon = -(c - cm_1)(c - cm_2),$$

$$\int_{\lambda}^{2\lambda} dx = \int_{c_f}^{c_0} \sigma \frac{dc}{-\frac{(c-c_1)(c-c_2)}{c} - \sigma B\epsilon},$$
$$\lambda = \int_{c_f}^{c_0} \sigma \frac{cdc}{-(c - cm_1)(c - cm_2)},$$

where

$$cm_1 = \frac{c_1 + c_2 - \sigma B\epsilon - \sqrt{(c_1 + c_2 - B\epsilon)^2 - 4c_1c_2}}{2}, \tag{3.14}$$
$$cm_2 = \frac{c_1 + c_2 - \sigma B\epsilon + \sqrt{(c_1 + c_2 - B\epsilon)^2 - 4c_1c_2}}{2}. \tag{3.15}$$

After expanding the integral equations(Eq.3.12-3.14), we obtain two equations related with λ, lowest speed(c_0), highest speed(c_f) and ϵ.

$$\lambda = -\frac{cp_1}{cp_1 - cp_2} \ln \frac{c_f - cp_1}{c_0 - cp_1} + \frac{cp_2}{cp_1 - cp_2} \ln \frac{c_f - cp_2}{c_0 - cp_2}. \tag{3.16}$$

$$\lambda = -\frac{cm_1}{cm_1 - cm_2} \ln \frac{c_0 - cm_1}{c_f - cm_1} + \frac{cm_2}{cm_1 - cm_2} \ln \frac{c_0 - cm_2}{c_f - cm_2}. \tag{3.17}$$

By Eq.3.16-3.17, we can get solutions of c_0 and c_f given ϵ and λ,

We performed simulations with "shocked region", initially firing region (shocked length = 1 unit). Neurons are set in one dimensional slice with discretization ($\delta = 1e - 3$). In the total domain, which is set to be 20, neurons are coupled through exponential function and decay exponentially. With constant alternating inhomogeneity, propagating speed is changing periodically due to the periodic inhomogeneity. Positive inhomogeneity increases the wave speed and the negative inhomogeneity decreases the wave speed. In one period, sustainable traveling wave depends on the value of ϵ and λ. Intuitively large perturbation amplitude and a long period of decreasing phase would cause propagation failure, when the speed is decreasing after every period and eventually reaches zero.

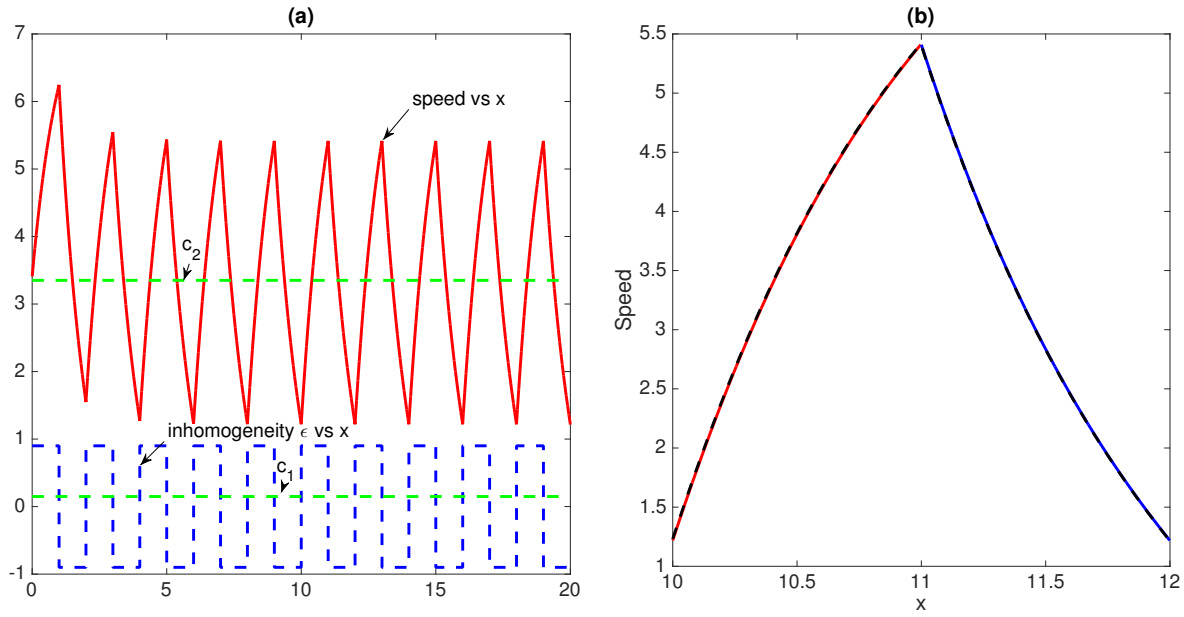

Figure (3.1) **Traveling wave speed with alternating inhomogeneity. (a) Speed changes with the constant inhomogeneity.** Red line denotes the propagating periodic speed versus space (x) under the influence of constant inhomogeneity $K(x)$ denoted by dashed blue line. **(b) Numerical simulation vs analytical solution** $x(c)$ **Eq.3.11.** Black line denotes numerical simulation result and red line is the wave speed when inhomogeneity equals ϵ, the other blue line is the wave speed when inhomogeneity equals $-\epsilon$. The parameters used here are: $\lambda = 1$, $\epsilon = 0.9$, $\tau_1 = 1$, $\tau_2 = 2$, $\sigma = 1$, $V_T = 1$, $g_{syn} = 10$, yielding $c_1 = 0.1492$ and $c_2 = 3.3508$. These parameters are used as default values, unless noted otherwise.

In Fig.3.1(a), we can see that traveling wave speed(red curve) changes in space(x), by the blue line of alternating constant homogeneity. Eventually it reaches stable periodic speed, where c_0, c_f denote the lowest point and highest point. Here with $\lambda = 1$, $\epsilon = 0.9$, $\tau_1 = 1$, $\tau_2 = 2$, $\sigma = 1$, $V_T = 1$, $g_{syn} = 10$, we can get $c_1 = 0.1492$, $c_2 = 3.3508$, and $c_0 = 1.22, c_f = 5.41$.

In Fig.3.1(b), analytical solution (Eq.3.11) from Fig.**??** is compared with numerical simulations, showing one period of excitation region($+\epsilon$) and one period of inhibition region($-\epsilon$) and they have a perfect agreement. Next, we performed simulations so that to confirm our

analytical solutions, and also reduced simulation time using our analytical product. In the numerical simulation, we used "shocked region", initially firing region (shocked length = 1 unit). Neurons are set in one dimensional slice with discretization ($\delta = 1e-3$). In the total domain, which is set to be 20, neurons are coupled through exponential function and decay exponentially. With constant alternating inhomogeneity, propagating speed is changing periodically by the inhomogeneity changing periodic (λ). Positive inhomogeneity increases the wave speed and the negative inhomogeneity decreases the wave speed. In one period, sustainable traveling wave depends on the value of ϵ and λ. Intuitively large perturbation amplitude and a long period of decreasing phase would cause propagation failure, when the speed is decreasing after every period and eventually reaches zero.

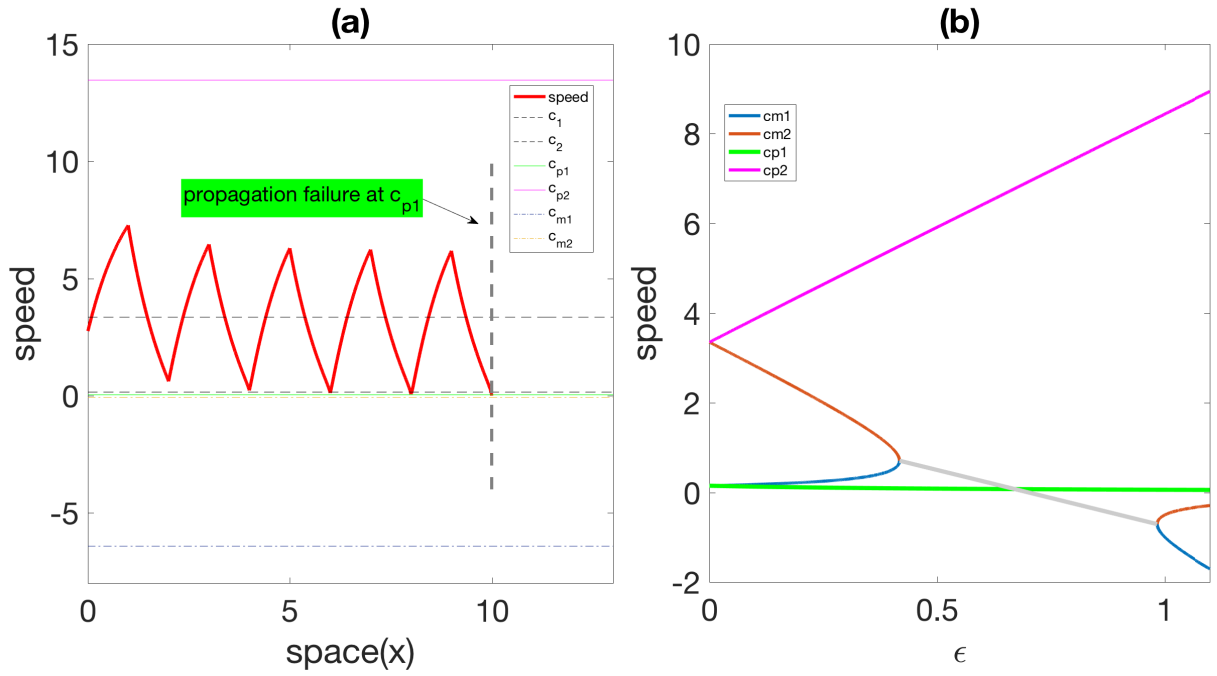

Figure (3.2) **Critical speeds in the constant periodic neural network.** (a) Critical speeds $(c_{p2}, c_{p1}, c_{m2}, c_{m1}, c_2, c_1)$ (Eq.[3.12, 3.14, 2.15]) in space. (b)Traveling wave critical speeds with increasing ϵ (Eq.3.12-Eq.3.14). Here $\lambda = 1$ is used. Magenta line is c_{p2}, green line is c_{p1}, red curve is c_{m2}, blue curve is c_{m1} and the grey line connects the negative and positive c_{m1}, c_{m2} which are imaginary when ϵ is between 0.42 and 0.98. When $\epsilon > 0.98$, the negative period suppress the propagation more and more, but when propagation failure occurs depends on the period length and if the speed is getting below c_{p1}.

We have a look at those critical speeds, $c_1, c_2, c_{p1}, c_{p2}, c_{m1}, c_{m2}$ with respect to x and ϵ and give explanations of how they affect the traveling wave speed(Fig.3.1-3.2). In Fig.3.2, when we use $\epsilon = 1.3$, traveling wave propagation(c_{tw}) fails at $x = 9.996$. In the positive region, c_{p1} and c_{p2} are the unstable and stable speed solution. During this period, if speed goes down of c_{p1}, propagation will definitely fail. While during the negative region, the unstable speed solution is c_{m1} and stable solution is c_{m2}. If the traveling wave speed gets lower that c_{m1} or if c_{m1} and c_{m2} are imaginary solutions, can we tell if propagation will fail?

Since the next period positive ϵ with bring up the speed, and only if the speed is greater

than c_{p1} after the negative period, the traveling wave propagation would not fail. when $lambda = 1$, the failure condition is $\epsilon > 1.31$, rather than bifurcation points in Fig.3.2.

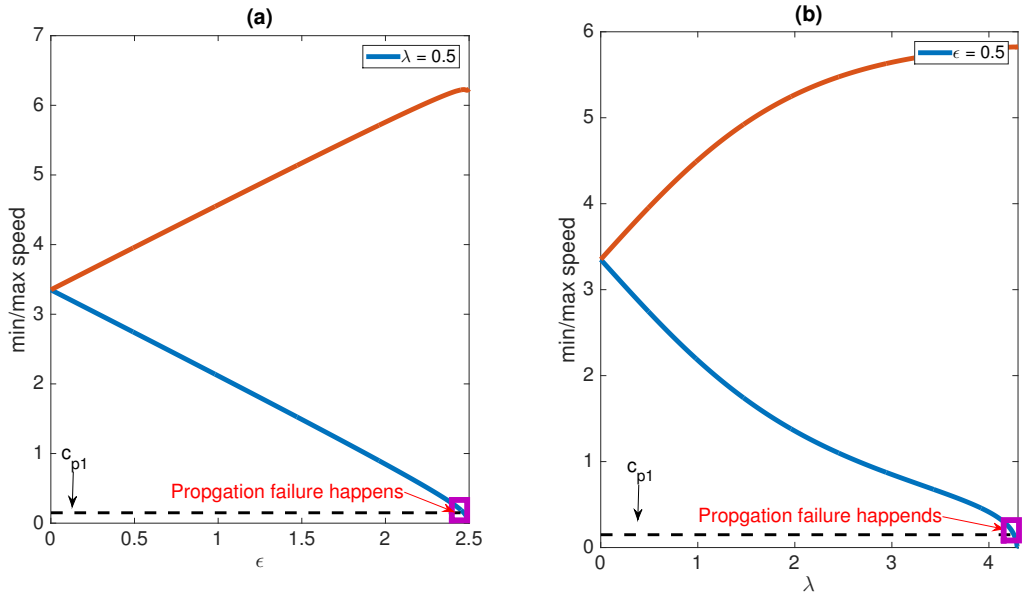

[]

Figure (3.3) **Traveling wave maximum/minimum speed (c_f/c_0) regarding to λ and ϵ. (a) Speed changes with λ fixed.** Red line denotes the maximum speed(c_f) while ϵ changes, and blue line is the minimum speed with fixed $\lambda = 0.5$ **(b) Speed changes with ϵ fixed.** Red line denotes the maximum speed while λ changes, and blue line is the minimum speed with fixed $\epsilon = 0.5$

Besides, Fig.3.3 gives us the graph of c_f/c_0 regarding to λ and ϵ. At $\epsilon = 0$ and $\lambda = 0$, the minimum and maximum of traveling wave speed are the same as the stable speed c_2. Increasing ϵ or λ, c_f and c_0 bifurcate, which means the oscillation gets larger and it is more prone to propagation failure. When the minimum speed gets smaller than c_p1, propagation failure will eventually occur. Fig.3.3(a) agrees with the blue dots (c_0, c_f) in Fig.3.3, when ϵ increases from 0 to the maximum $\epsilon = 1.31$ with $\lambda = 1$ in alternating constant inhomogeneous network.

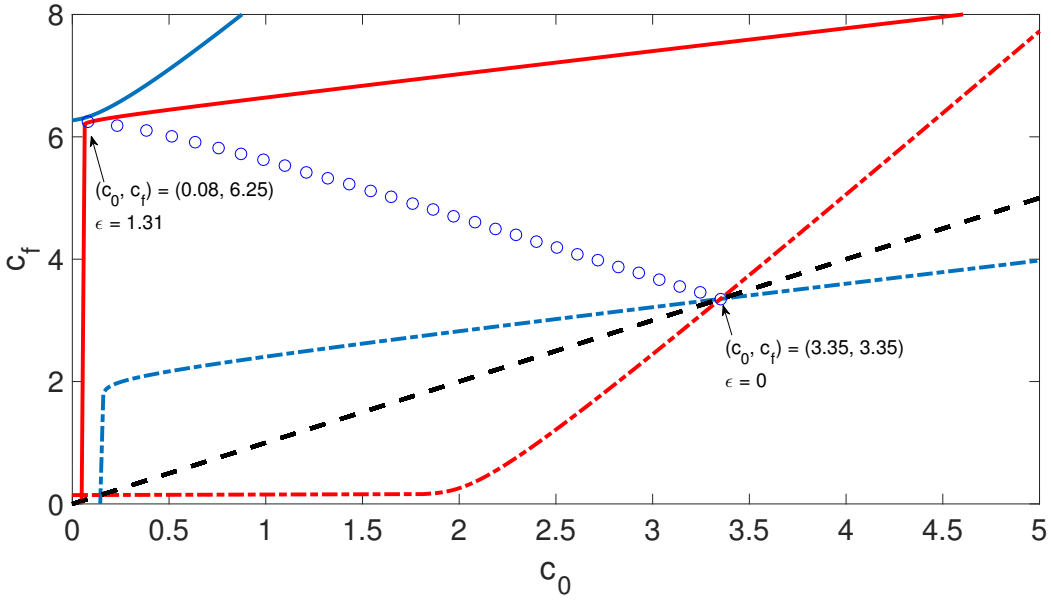

Figure (3.4) **Dynamics of propagation failure with uniform regions of excitation and inhibition(Eq. 3.16-3.17).** The black line is $y = x$, when $\epsilon = 0$, the traveling wave speed is a constant value. The red dash line and the blue dash line are from equations 3.16-3.17 when $\epsilon = 0$, the constant speed $c_2 = c_0 = c_f = 3.35$. When the ϵ increases, the solutions for c_0 and c_f are denoted by blue circles. Up to the point that blue and red lines is to separate, that is, $c_0 = 0.08, c_f = 6.25, \epsilon = 1.31$, propagation will fail. $\lambda = 1$ is used here.

As a simple example of periodic inhomogeneity in integrate-and-fire neural network, the alternating constant inhomogeneity by changing period λ, the amplitude of inhomogeneity is constant ϵ. $c_{p1}(3.12)$ is the cross-line of propagation failure. Besides, the traveling wave speed oscillates around speed c_2, the larger ϵ and λ, the more traveling wave speed oscillates.

The more complicated case is when the inhomogeneity value is changing every location, and our guess is that the c_2 is not any more the periodic speed oscillates around. In the next section, we will dig further on the cosine periodic inhomogeneity effect on traveling wave propagation in one-dimensional integrate-and-fire neural network.

3.3 Illustration of propagation failure with non-constant periodic inhomogeneity

By the result of Eq. 3.7, $K(x)$ is the perturbation function that affects the activities of traveling waves. If we take the periodic inhomogeneity in the form of cosine function, that is, $K(x) = \epsilon \cos(\omega y)$, where ϵ controls the amplitude of the perturbation, and ω denotes the frequency of periodic change and one period equals $\lambda = 2\pi/\omega$. Here is our equation for the traveling wave propagation acceleration as a function of speed under the influence of periodic cosine inhomogeneity.

$$a(x) = -\frac{(c(x) - c_1)(c(x) - c_2)}{\sigma} + \frac{gc(x)}{2V_T\tau_1}\epsilon \cos(\omega x) \tag{3.18}$$

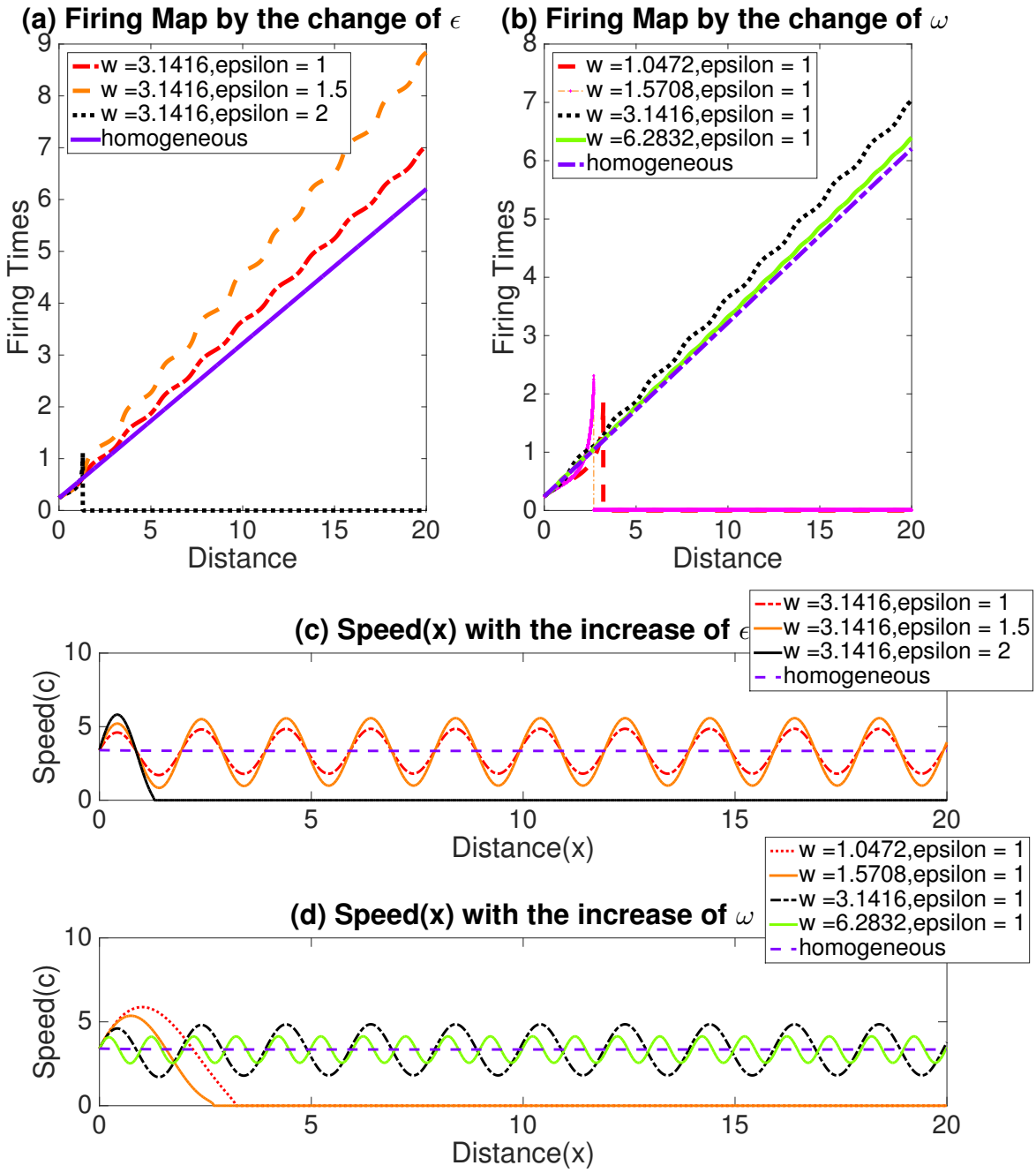

Figure (3.5) **Firing maps and numerical simulation of propagating speed of traveling waves with the change of ϵ and ω.** (a) (c). By fixing ω and increasing ϵ, traveling wave oscillates wider and wider and eventually it induces propagation failure. (b) (d). By fixing ϵ and decreasing ω, traveling wave oscillates more frequently and gets more likely suppressed by inhomogeneities. The parameters used here are: $\tau_1 = 1, \tau_2 = 2, \sigma = 1, V_T = 1, g = 10$, yielding $c_1 = 0.1492$ and $c_2 = 3.3508$. These parameters are used as default values, unless noted otherwise.

From Fig. 3.6, we can tell that ϵ and ω together affect the propagation activities of traveling waves. Figure 3.6(a-b) are firing maps by the change of ϵ and the change of ω separately. We can tell that It is getting easier to stop propagation with larger ϵ and smaller of ω, or larger wavelength (λ). Figure 3.6(c-d) show the speed versus space, with the change ϵ and ω. Traveling wave speed shows a periodic wave. The period is fixed or controlled by the value of ω.

From the perspective synaptic connectivity, the coupling function has changed due to periodic inhomogeneity. Figure **??** has illustrated how the inhomogeneity affects the synaptic connectivity.

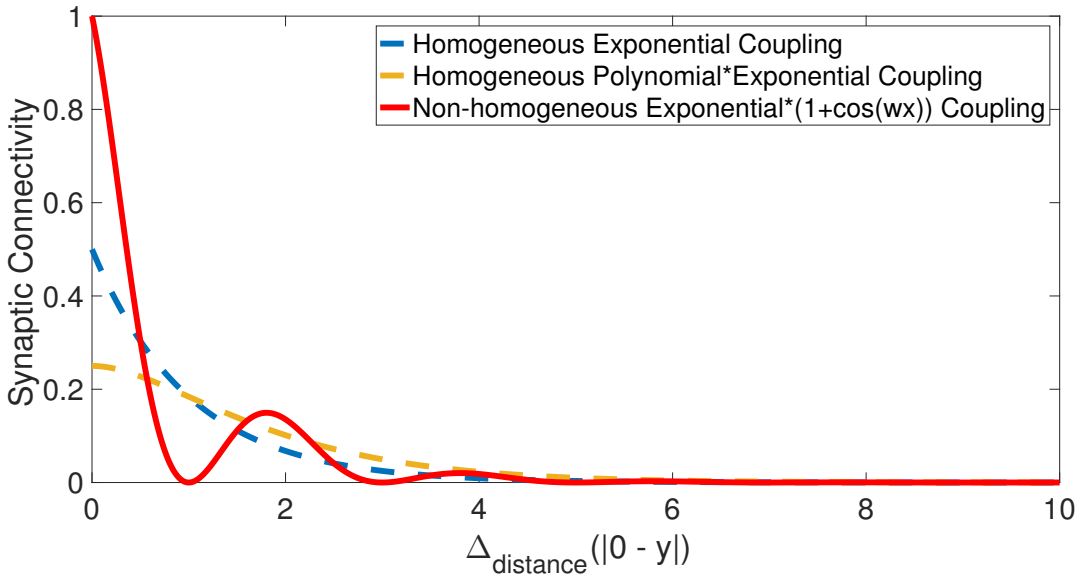

Figure (3.6) **Synaptic coupling function influenced by periodic inhomogeneity.** The blue curve and orange curve are homogeneous coupling functions. When the network is influenced by periodic inhomogeneities, the synaptic connectivity also shows a damping oscillation of the distance between neurons. Here the synaptic connectivity is for the neuron at location $x = 0$ and y.

The next question is what are the critical speeds that could induce propagation failure. Also analytical solutions or asymptotic solutions are our main research targets in the

following sections.

Numerically, we can utilize the initial differential equation (3.10) and shoot an initial speed and then observe what the speed approaches towards and determine if it finally becomes stable or fails eventually. c_1 is the unstable speed in the homogeneous network. Two inhomogeneity related parameters: ϵ and ω will be studied, which together affect the propagation of traveling waves. It is getting easier to stop propagation with larger ϵ and smaller of ω, or larger wavelength (λ). In Fig.3.7, with three initial shooting speed, $c = 0.50, c = 0.45, c = 0.40$, the ϵ range for sustainable traveling wave propagation will shrink with a smaller initial speed. Here parameters we used are $\tau_1 = 1, \tau_2 = 2, \sigma = 1, V_T = 1, g_{syn} = 6$, so that we have our constant speed solutions $c_1 = 0.5$ and $c_2 = 1.0$ in homogeneous medium. By that, when the initial shooting speed is $c = 0.3812$, only $\epsilon = 0.2653$ traveling wave will have a stable speed, otherwise, propagation fails.

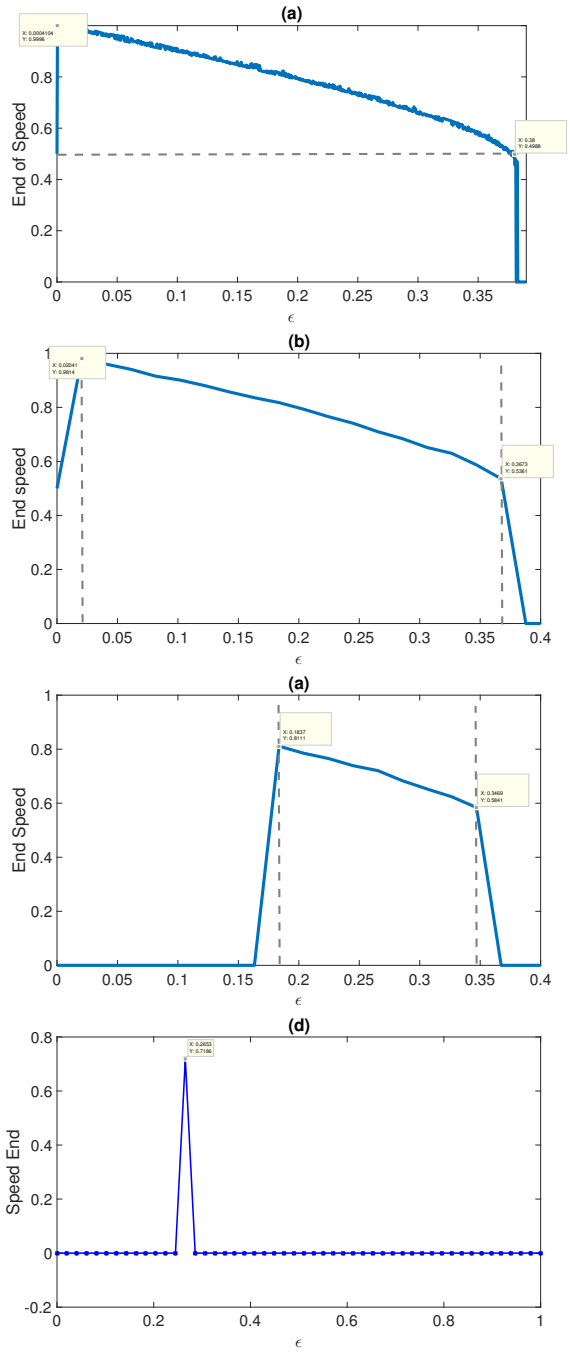

Figure (3.7) **Traveling wave speed with different initial shooting speed for numerical simulation for 100 periods.** (a) Initial shooting speed: $c_0 = 0.50$. The range of traveling propagating ϵ is $[0.0, 0.38]$. (b) Initial shooting speed: $c_0 = 0.45$. The range of traveling propagating ϵ is $[0.0204, 0.3673]$. (c) Initial shooting speed: $c_0 = 0.40$. The range of traveling propagating ϵ is $[0.1837, 0.3469]$. (d) Initial shooting speed: $c_0 = 0.3812$. The range of traveling propagating ϵ is $[0.2653, 0.2653]$. The parameters used here are: $\tau_1 = 1, \tau_2 = 2, \sigma = 1, V_T = 1, g_{syn} = 6$, yielding $c_1 = 0.5$ and $c_2 = 1.0$. These parameters are used as default values, unless noted otherwise.

3.4 Speed approximations of traveling Wave Speed

It becomes complicated to obtain implicit speed solutions from non-constant periodic inhomogeneous neural network.

Initially, we consider c_2 is the speed that the traveling wave oscillates around. However, it is not the case. we conducted simulation about how the center speed changes with ϵ in the case that $c_1 = 0.5, c_2 = 1$. Obviously, the center speed or the stable speed solution is not fixed at 1, instead, it is changes from $c_2 = 1$ to a speed($c = 0.84$) with the increase of ϵ]. The result is different from the homogeneous case and also the constant inhomogeneous neural network. This result is also consistent with figure 3.7 that when ϵ exceeds 0.38, there would eventually cause propagation failure losing stable speed solution. Here we discussed the results with rounded values to two decimal places.

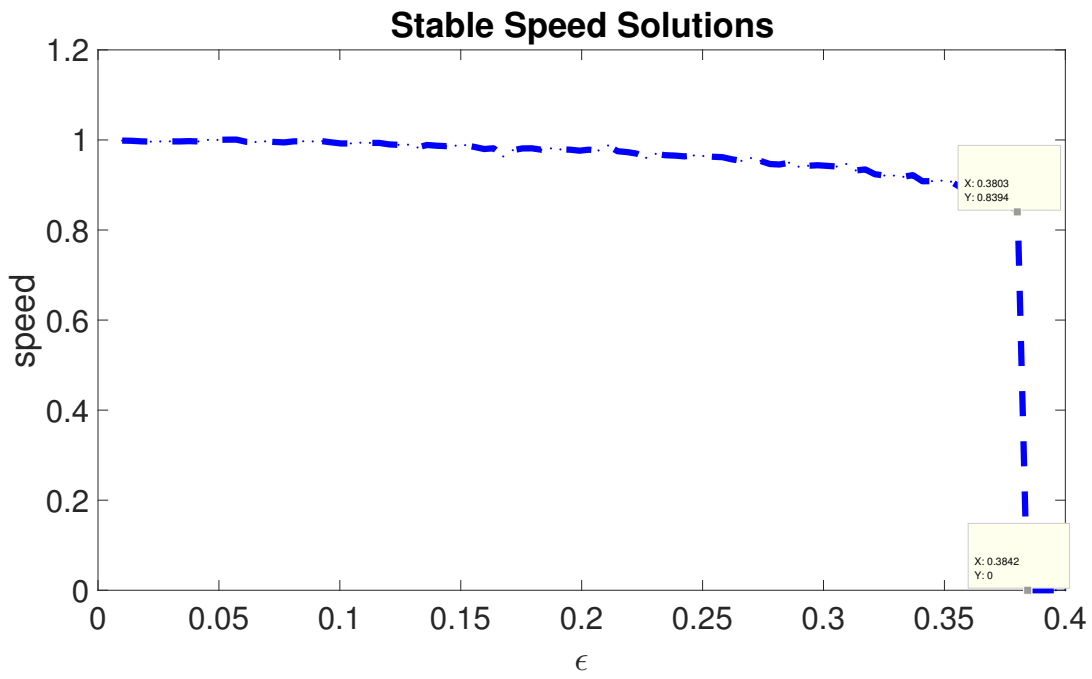

Figure (3.8) **Stable speed solution or the speed oscillating around with the increase of ϵ.** The speed that the traveling wave oscillates around is changing from rom $c_2 = 1$ to a speed($c = 0.84$) with the increase of ϵ] from 0 to 0.38. When $epsilon = 0$ is exact the homogeneous neural network, when the speed centered is $c_2 = 1$. It also shows that the maximum $epsilon = 0.38$. Here we have rounded our results to two decimals.

Therefore, we start to consider the traveling wave speed in the form of

$$v = a_0 + a_1 cos(\omega x) + a_2 sin(\omega x). \tag{3.19}$$

a_0, a_1, a_2 are our parameters that need to be clarified. In one period, we take $x = 0, \pi/\omega, \pi/\omega$, so that we can obtain three equations containing three parameters(a_0, a_1, a_2). Here is our vector form of speed and the derivative of speed dv/dx by using $x = 0, \pi/\omega, \pi/\omega$.

$$v = [a_0 + a_1; a_0 + a_2; a_0 - a_1], \tag{3.20}$$

$$\frac{dv}{dx} = [\omega a_2; -\omega a_1; \omega a_1]. \tag{3.21}$$

Thus we can substitute v and v' in equation 3.10, and obtain that

$$a_0 = 0.9474, \tag{3.22}$$

$$a_2 = -0.2813, \tag{3.23}$$

$$a_3 = 0.03577. \tag{3.24}$$

with $\epsilon = 3, g_{syn} = 6, \omega = \pi$. Thus our speed approximation to

$$c(x) = 0.9474 - 0.2813cos(\pi x) + 0.03577sin(\pi x). \tag{3.25}$$

The fit has a very small RMSE that we could believe that speed approximation is almost perfect good, as shown in figure 3.9. In this way, we can estimate our propagation speed analytically and numerically.

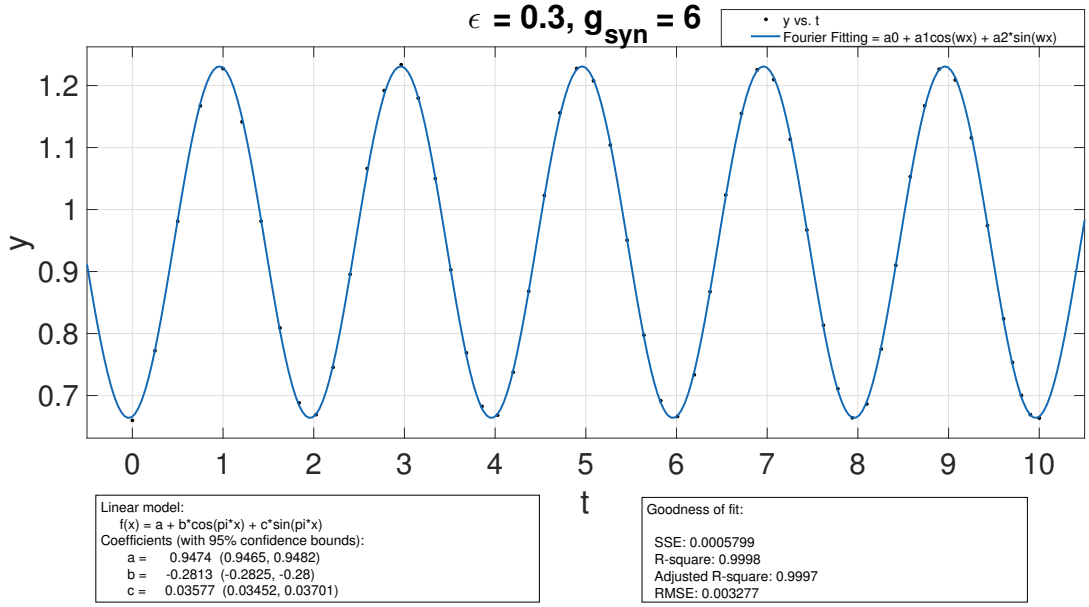

Figure (3.9) **Propagating speed approximation.** The results show an almost perfect fit with our analytical equations for traveling wave speed(Eq.3.25) with a quite small mean square error.

However, for a fast traveling wave, the inhomogeneity is small that $\epsilon \leq 0.1$, the speed of traveling wave keeps around the stable state (c_2) , which could be described as a series of perturbation terms as follows,

$$c = c_2 + \epsilon h_1(x) + \epsilon^2 h_2(x) + ... + \epsilon^n h_n(x) + ... \tag{3.26}$$

where ϵ is the amplitude of the periodic inhomogeneities and the higher-order terms in the series become successively smaller and smaller.

Also, by Taylor's expansion,

$$\begin{aligned}\frac{1}{c(x)} = \quad & \frac{1}{c_2} - \frac{h_1}{c_2^2}\epsilon + (\frac{h_1^2}{c_2^3} - \frac{h_2}{c_2^2})\epsilon^2 - \\ & (\frac{1}{c_2^4}h_1^3 - \frac{2}{c_2^3}h_1 h_2 + \frac{1}{c_2^2}h_3)\epsilon^3 + R_3(\epsilon),\end{aligned}$$

where $R_3(\epsilon)$ is the remainder of the taylor's series, which approximates to zero. Thus, Eq. 3.26 can be rewritten into

$$\sigma\frac{dc}{dx} = -c + c_1 + c_2 - c_1c_2(\frac{1}{c_2} - \frac{1}{c_2^2}h_1(x)\epsilon +$$
$$(\frac{1}{c_2^3}h_1^2 - \frac{1}{c_2^2}h_2)\epsilon^2 - (\frac{1}{c_2^4}h_1^3 - \frac{2}{c_2^3}h_1h_2 + \frac{1}{c_2^2}h_3)\epsilon^3) + \sigma B\epsilon cos(\omega x).$$

Solvable differential equations thus are established for the series of perturbation terms $(h_1(x), h_2(x), h_3(x))$, let $\lambda_0 = -(c_2 - c_1)/c_2$, we obtain the following ordinary differential equations for $h_1, h_2 and h_3$, we can also list the general form to solve h term similarly, so that we can go higher order of approximation if needed.

$$\sigma h_1'(x) = \lambda_0 h_1(x) + \sigma B\cos(\omega x),$$
$$\sigma h_2'(x) = \lambda_0 h_2(x) - \frac{c_1}{c_2^2}h_1^2,$$
$$\sigma h_3'(x) = \lambda_0 h_3(x) + \frac{c_1}{c_2^3}h_1^3 - \frac{2c_1}{c_2^2}h_1h_2.$$

As a result, $h_1(x), h_2(x), h_3(x)$ take the following trigonometric form,

$$h_1(x) = A_1\cos(\omega x + \phi_1),$$
$$h_2(x) = A_2\cos(2\omega x + \phi_2) + C_1,$$
$$h_3(x) = A_3\cos(\omega x + \phi_3) + A_4\cos(3\omega x + \phi_4),$$

where

$$
\begin{aligned}
A_1 &= \sigma B/\sqrt{\lambda_0^2 + (\sigma\omega)^2}, \\
\phi_1 &= -\arccos\left(\lambda_0/\sqrt{\lambda_0^2 + (\sigma\omega)^2}\right), \\
A_2 &= -c_1 A_1^2/2c_2^2\sqrt{\lambda_0^2 + (2\sigma\omega)^2}, \\
\phi_2 &= 2\phi_1 - \arccos\left(\lambda_0/\sqrt{\lambda_0^2 + (2\sigma\omega)^2}\right), \\
C_1 &= -c_1 A_1^2/(2c_2^2\lambda_0), \\
B &= g_{syn}/(2V_t\tau_1),
\end{aligned}
$$

You can find details of the analytical results of $(A_3, A_4, \phi_3, \phi_4)$ in the appendix. We do not put here since they have a long form and will not be analyzed any further. The results are illustrated in figure 3.10

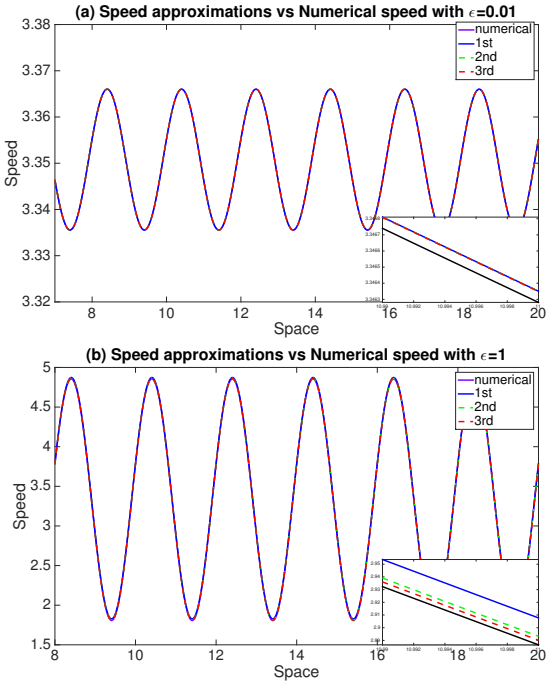

Figure (3.10) **Speed Approximations vs Numerical Simulations.** By the analytical results, first order, second order and third order approximations of speed are plotted compared with the results from numerical simulations. A subfigure is plotted in bottom right which shows the zoomed region $x = 10.9900 : 11.0000$. (a). $\epsilon = 0.01$. (b) $\epsilon = 1$. Here $\omega = \pi$ is used.

We can tell from Fig. 3.10(a) when $\epsilon \leq 0.01$ is very small, the first order approximation is pretty good to approximate the speed. With a larger $\epsilon = 1$(Fig. **??**(a)), the assumption does not hold any more.

3.5 Induction of traveling wave speed

We can see from the solutions that h_1 has frequency ω, h_2 has frequency 2ω and constant, h_3 has frequency 3ω and ω, thus we made the following assumptions:

$$h_{2n} = \sum_{j=0}^{n} A_{2nj} cos(2jwx + \phi_{2nj}).$$
$$h_{2n+1} = \sum_{j=0}^{n} A_{(2n+1)j} cos((2j+1)wx + \phi_{(2n+1)j}).$$

This assumption needs to be confirmed through the who[Speed approximations vs numerical simulations] le space. As we've explained above, each $h(x)$ has an expressive equation in general,

$$\sigma h_k' = -h_k - \frac{c_1 c_2 (1/c)^{(k)}(\epsilon = 0)}{k!}, k = 2, 3, 4... \tag{3.27}$$

$$\begin{aligned}
&\frac{1}{c}^{(1)}(\epsilon = 0) = f_1(h_1) \\
&\frac{1}{c}^{(2)}(\epsilon = 0) = f_2(h_1^2, h_2) \\
&\frac{1}{c}^{(3)}(\epsilon = 0) = f_3(h_1^3, h_1 h_2, h_3) \\
&\frac{1}{c}^{(4)}(\epsilon = 0) = f_4(h_1^4, h_1^2 h_2, h_2^2, h_1 h_3, h_4) \\
&\qquad\qquad ...
\end{aligned}$$

Where $(1/c)^{(k)}(\epsilon = 0)/k!$ is a sum of terms $(h_i^{k_i} h_j^{k_j})$, satisfying $ik_i + jk_j = k, 0 \leq i, j \leq k, h_0 = 1$. For example: when $k = 2, (1/c)^{(2)}(\epsilon = 0)$ is a combination of $h_1 h_2, h_1^3, h_3$. A sum of those terms has the notation $f_k(h_i^{k_i} h_j^{k_j})$, thus,

$$\sigma h_k' = -h_k - c_1 c_2 f_k(h_i^{k_i} h_j^{k_j}) \tag{3.28}$$

Then by Eq. 3.28,

$$\sigma h_{2n+2}' = -h_{2n+2} - c_1 c_2 f_{2n+2}(h_i^{k_i} h_j^{k_j}) \tag{3.29}$$
$$\sigma h_{2n+3}' = -h_{2n+3} - c_1 c_2 f_{2n+3}(h_a^{k_a} h_b^{k_b}) \tag{3.30}$$

where $ik_i + jk_j = 2n+2, ak_a + bk_b = 2n+3, 0 \le i,j \le 2n+2, 0 \le m,n \le 2n+3, h_0 = 1$.

By the properties of cosine functions,

if mn is even,

$$cos(mwx)^n = \sum_{j=0}^{mn/2} B_{1j} cos(2jwx),$$

if mn is odd,

$$cos(mwx)^n = \sum_{j=0}^{(mn-1)/2} B_{2j} cos((2j+1)wx),$$

if $m+n$ is even,

$$cos(mwx)cos(nwx) = \sum_{j=0}^{(m+n)/2} B_{3j} cos(2jwx),$$

if $m+n$ is odd,

$$cos(mwx)^n = \sum_{j=0}^{(m+n-1)/2} B_{4j} cos((2j+1)wx),$$

where B_{ij} are constant coefficients.

Thus we can get the general form about $h_i^{k_i} h_j^{k_j}$ with $ik_i + jk_j = 2n+2$,

if both ik_i and jk_j are odd,

$$\begin{aligned} h_i^{k_i} h_j^{k_j} = & \sum_{j=0}^{(ik_i-1)/2} A_{1j} cos((2j+1)wx) \cdot \\ & \sum_{j=0}^{(jk_j-1)/2} A_{2j} cos((2j+1)wx) \\ = & \sum_{j=0}^{n+1} A_{3j} cos(2jwx). \end{aligned}$$

Similarly if both ik_i and jk_j are even,

$$h_i^{k_i} h_j^{k_j} = \sum_{j=0}^{ik_i/2} A_{1j} cos((2j)wx) \sum_{j=0}^{jk_j/2} A_{2j} cos((2j)wx)$$
$$= \sum_{j=0}^{n+1} A_{3j} cos(2jwx).$$

Therefore,

$$h_i^{k_i} h_j^{k_j} = \sum_{j=0}^{n+1} A_{4j} cos(2jwx).$$

Similarly,

$$h_a^{k_a} h_b^{k_b} = \sum_{j=0}^{n+1} A_{5j} cos((2j+1)wx).$$

The solutions for h_{2n+2}, h_{2n+3} from Eq. 3.30-3.30 become

$$h_{2n+2} = \sum_{j=0}^{n+1} A_{(2n+2)j} cos(2jwx + \phi_{(2n+2)j}).$$
$$h_{2n+3} = \sum_{j=0}^{n+1} A_{(2n+3)j} cos((2j+1)wx + \phi_{(2n+3)j}).$$

Therefore, by induction we confirmed the generic analytical speed approximation is,

$$c = c_2 + h_1\epsilon + h_2\epsilon^2 + h_3\epsilon^3 + ...$$

where

$$h_{2n} = \sum_{j=0}^{n} A_{2nj} cos(2jwx + \phi_{2nj}).$$
$$h_{2n+1} = \sum_{j=0}^{n} A_{(2n+1)j} cos((2j+1)wx + \phi_{(2n+1)j}).$$

In general, we can have a good approximation of traveling wave speed by taking more terms with higher order of ϵ, but with one condition that it is a fast traveling wave and ϵ is relatively small, also we compared with numerical simulation (ODE45) as shown in figure 3.11. In this way, we can visualize higher order approximations easily when the mathematical expression becomes crazy long and complicated. It is faster to get a good speed approximation compared to simulate from the original evolution equation.

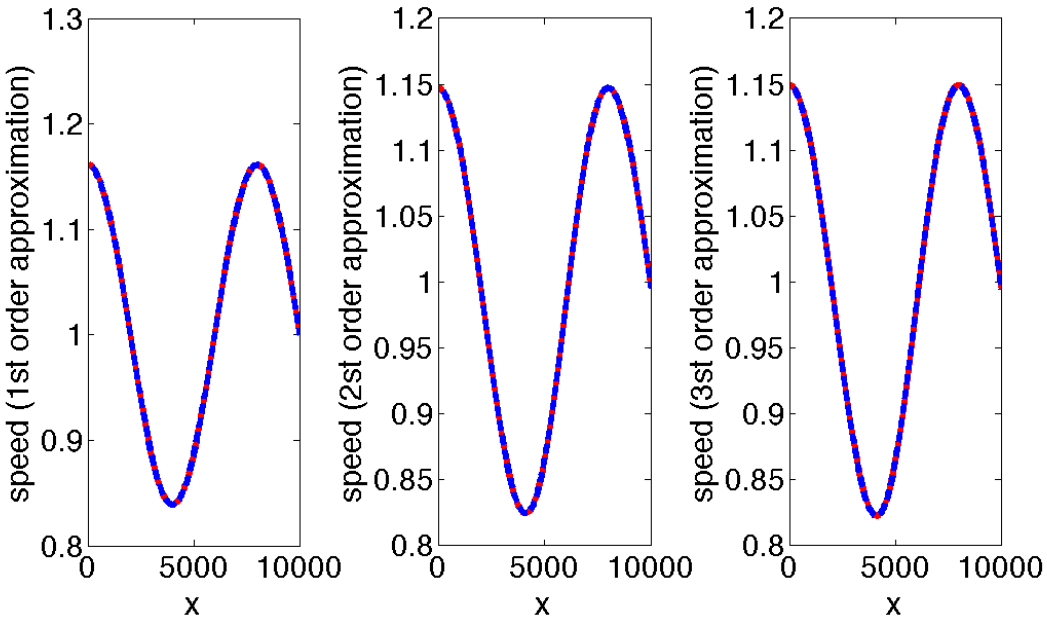

Figure (3.11) **Numerical simulation with ODE45 with the analytical approximations of traveling wave speed.**

(a) First order approximation. (b) The second order approximation. (c) The third order approximation. Numerically we can use our series of speed approximations to help us visualize the speed of activities of traveling wave propagation.

3.6 Conditions Inducing propagation Failure

By knowing that the traveling wave speed could be approximated with equation 3.25, we manage to find the conditions when propagation failure occurs, because the critical speed

is not any more a constant value, instead, it is a changing value over the value of ϵ.

We conduct simulations on how the maximum speed (c_f) changes with the minimum speed(c_0). The time length between the c_f and c_0 is λ. When it is a homogeneous neural network,

$$c_0 = c_f, \tag{3.31}$$

as a constant speed solution, which equals c_2. Figure 3.12 shows the relationship between c_f and c_0 regarding to different values of ϵ.

In Fig. 3.12, three examples of *epsilon* are plotted, as $\epsilon = 0.29$, there two interaction points with line $y = x$, which means that there are two speed solutions, and the largest one is the stable speed that the traveling wave speed would oscillate around this value. When ϵ increases and reaches $\epsilon = 0.3822$, there is only one interaction point and traveling wave is going to lose stability. So as an example of failure propagation, when $\epsilon = 0.50$, no stability could be reached.

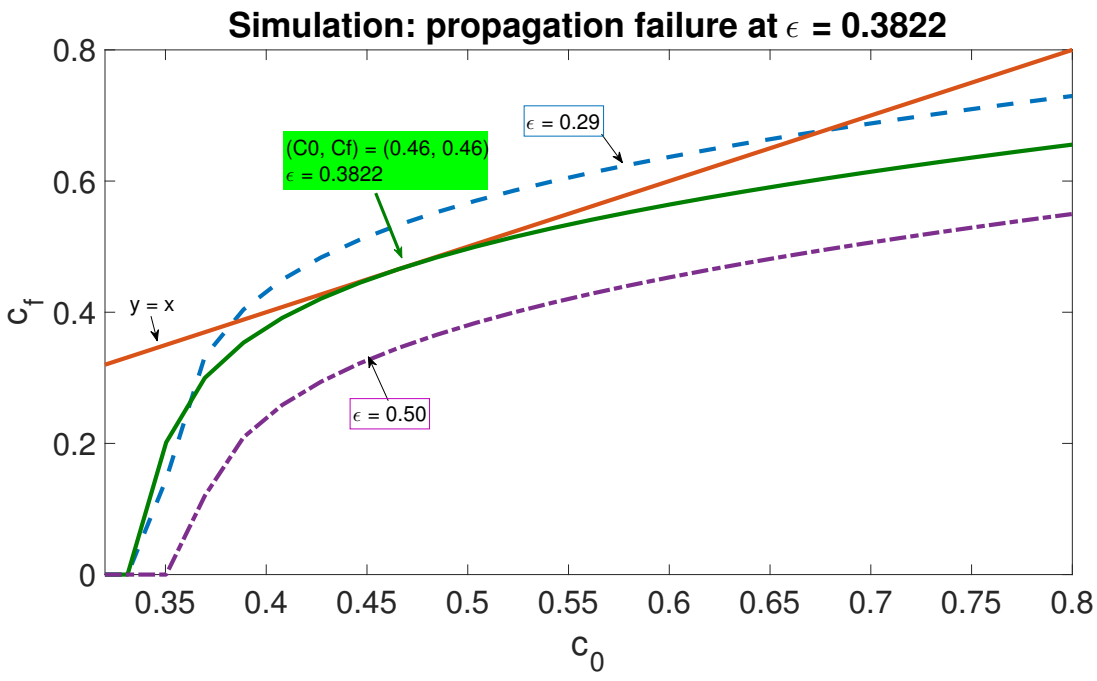

Figure (3.12) **Propagation failure simulation at different ϵ.** Red curve denotes the line $y = x$, when the stability could be reached. blue line is when $\epsilon = 0.29$, propagation could reach stability to the stable solution(the larger interaction point). However, when we increase ϵ, the two solutions would collide into one, when $\epsilon = 0.3822$, the traveling wave propagation is going to lose stability as in the example of $\epsilon = 0.50$, there is no way realizing a stable traveling wave propagation.

In summary, in the inhomogeneous neural network, we looked two types of inhomogeneity, constant periodic function and cosine function. In both cases, traveling wave speed would oscillate around a stable speed, if *epsilon* increases too large or the traveling wave period is two small, propagation would fail. Analytically we can find and prove that the critical speed inducing propagation failure is c_{p1} rather than c_1 ($c_{p1} < c_1$).

However, in the cosine inhomogeneity, it is not a constant critical speed inducing propagation failure. Figure 3.8 gives us the changing of stable speed regarding to different ϵ. The stable speed is changing with ϵ. We have simulated and approximated speed with the mathematical form(Eg.3.25), which shows an excellent goodness of fit. Furthermore, we simulate

the dynamics of how the system loses stability due to the increase of ϵ.

CHAPTER 4

CONCLUSIONS

In conclusion, for a specific class of Integrate-and-Fire neural networks that neurons are exponentially connected, it is analytical solved that the instantaneous acceleration depends only on a quadratic function of the instantaneous speed of the traveling wave propagation, analytically rendering two speed solutions: one is slow-unstable and the other is fast-stable. This is a powerful and surprising result since in principle each neural spike influences the rest of the network, and would seemingly need to be accounted when solving for the exact network dynamics. This quadratic dependence on speed provides a clear explanation of why this type of neural network can sustain two types of traveling waves, a slow-unstable wave as well as a fast-stable wave, while ruling out other possible solutions.

Furthermore, this approach provides a global explanation of the traveling wave stability. When the propagation dips below the slow-unstable speed c_1, a negative acceleration will further reduce the speed until the propagation fails. In contrast, the propagation speeds up or down toward the fast-stable traveling wave c_2, depending if the initial speed is below or above c_2 respectively. It is not possible to achieve this level of insight into the stability of traveling waves for other models since the proofs of their stability rely on perturbation theory.

Another fundamental result of this type of model is that evolution toward propagation failure or constant speed traveling wave is determined by a natural global timescale that depends only on the neuron integration time τ_1, the time constant for the decay of the excitation τ_2, and on the ratio between the global excitation constant g_{syn} and the voltage threshold V_t. This provides us an easy way of quantifying how fast do dynamics of neural spikes evolve toward the stable states of either propagation failure or constant speed traveling waves.

Not only limited to homogeneous network, the analytical methods can also be used to derive conditions for propagation failure in the presence of a non-conductive gap. Not surprisingly, a small to moderate gap reduces the speed of the propagation by an amount that is small enough to allow recovery toward the fast-stable traveling waves. In contrast, a large gap would either block propagation altogether, or would result in a wave that jumps the gap but has a speed that is below the slow-unstable solution and it will eventually fail.

In addition to exponential synaptic connectivity, these results can be extended for more general kernels, provided that the derivatives of the spatial and temporal kernels generate a finite set of functions. Under these assumptions, the evolution equations for the propagation of activity in the neural network can be converted to a system of ordinary differential equations with dynamics depending on the local conditions. Those local conditions are derived from a finite number of derivatives of the firing map $t(x)$. It is fascinating that despite the long-range connections considered in these models, the evolution of these waves follows local rules for their dynamics. It is also quite unexpected that this is the case for longer-range kernel such as exponential functions, but not for the more compact kernels such as Gaussian functions, since naively it would seem that the longer the range the more likely a neuron spike would influence the dynamics of the whole network.

Not only improving our insight into the mechanism of these traveling waves, but also this approach has the potential to significantly improve the simulation times for large-scale networks. Instead of maintaining the state of all neurons in the working memory during simulations, one needs to simulate only a system of ordinary differential equations for the position of the traveling wave-front, resulting in substantial reduction of the simulation times.

Additionally, we can derive analytical equations for multiple spiking neural networks, providing the relationship between propagation acceleration as a function of speed. However, it is challenging to obtain further analytical results from the multiple spiking neural networks. Furthermore, inhomogeneities, where the dynamics described are subject to modulations induced by additional weak and non-homogeneous kernels. Two special types of kernels are discussed: uniform additional excitation and inhibition, and continuous cosine function.

Under the influence of the additional uniform excitation and inhibition, traveling wave speed behaves periodic. The larger of the inhomogeneous amplitude, or the smaller frequency of oscillation, it is getting easier to propagation failure. Through integrating the analytical expression of acceleration as a function of speed, two critical traveling wave speed solutions are obtained when there is additional excitation. In this case, the stable speed(c_{p2}) is increased, while the unstable speed(c_{p1}) is decreased below c_1. When the inhomogeneity changes to uniform inhibition, there are two new critical speed solutions, which can bring the traveling wave speed to a new stable state or it is all the way decreasing if the speed is less than the slow-unstable speed. By larger amplitude of inhibition, the effect of synaptic inhibition becomes so pronounced that the wave speed is decreasing faster. After one period, the network changes to synaptic excitation; However, the propagation can still fail provided that the instantaneous speed falls below c_{p1}. In summary, we have explored the dynamics of traveling wave propagation stability changes over space and time, as well as the period(λ) and the amplitude of the inhomogeneity(ϵ).

However, it is not easy for the cosine inhomogeneous network to derive a mathematical expression of analytical speed solutions. We can no longer define a fixed critical speed as the effect of inhomogeneities are changing over locations. Numerically we can explain how the speed changes with ϵ and how the system loses stability. Contrary to the homogeneous network, we discovered from numerical simulations that c_1 is not the minimum speed that the traveling wave can sustain, and c_2 is not the average speed for activity propagation. But with the assumption of small and periodic inhomogeneity modulation, we can construct a series of speed approximations and get more accurate speed estimates with higher order terms of ϵ.

Furthermore, we could fit the traveling wave speed in a linear form of cosine term and sine term, which turns out to be an excellent fit with a quite small mean square error. The challenge here is that we need a way to determine the initial conditions. The cosine form inhomogeneity has involved changing speed solutions by locations. Compared with the homogeneous neural network, inhomogeneous neural network in continuous cosine form

could allow the traveling wave speed to reach a value smaller than c_1 without achieving propagation failure. Through analytical results and numerical simulations, the minimum ϵ value can be determined for neural network traveling wave propagation.

In the future, I am interested in extending the analytical methods to more complex models and translate these results into two-dimensional networks. Also, we can consider including both excitatory and inhibitory neurons to the network according to real biological scenarios, not only periodically changing inhomogeneities. More ideally, we can apply our methods to analyze experimental data of traveling wave electrical activities to determine the traveling wave speed, the transition between wave propagation success and failure, and also the conditions inducing propagation failure.

REFERENCES

[1] Tatsuo K. Sato, Ian Nauhaus, and Matteo Carandini. Traveling waves in visual cortex. *Neuron*, 75(2):218–229, 2012.

[2] Tim Wanger, Kentaroh Takagaki, Michael T Lippert, Jurgen Goldschmidt, and Frank W Ohl. Wave propagation of cortical population activity under urethane anesthesia is state dependent. *BMC Neurosci.*, 14:78, 2013.

[3] James B Ackman and Michael C Crair. Role of emergent neural activity in visual map development. *Current Opinion in Neurobiology*, 24:166–175, 2014.

[4] James B. Ackman, Timothy J. Burbridge, and Michael C. Crair. Retinal waves coordinate patterned activity throughout the developing visual system. *Nature*, 490(7419):219–25, 2012.

[5] Theodoros P. Zanos, Patrick J. Mineault, Konstantinos T. Nasiotis, Daniel Guitton, and Christopher C. Pack. A sensorimotor role for traveling waves in primate visual cortex. *Neuron*, 85:615–627, 2015.

[6] Ian Nauhaus, Laura Busse, Dario L. Ringach, and Matteo Carandini. Robustness of traveling waves in ongoing activity of visual cortex. *Journal of Neuroscience*, 32(9):3088–94, 2012.

[7] Albert Compte, Maria V. Sanchez-Vives, David A. McCormick, and Xiao-Jing Wang. Cellular and network mechanisms of slow oscillatory activity (¡1hz) and wave propagations in a cortical network model. *Journal of Neuropysiology*, 89:2707–2725, 2003.

[8] M. Murakami, H. Kashiwadani, Y. Kirino, and K. Mori. State-dependent sensory gating in olfactory cortex. *Neuron*, 46(2):285–296, 2005.

[9] A. Reimer, P. Hubka, A. K. Engel, and A. Kral. Fast propagating waves within the rodent auditory cortex. *Cerebral Cortex*, 21(1):166–177, 2011.

[10] M. Chrostowski, L. Yang, H. R. Wilson, I. C. Brue, and S. Becker. Can homeostatic plasticity in deafferented primary auditory cortex lead to traveling waves of excitation? *J. Comput Neurosci.*, 30(2):279–99, 2011.

[11] D. R. Belov, P. A. Stepanova, and S. F. Kolodyazhnyi. Traveling waves in the human eeg during voluntary hand movements. *Neuroscience and Behavioral Physiology*, 45:1–12, 2015.

[12] D. Rubino, K. A. Robbins, and N. G. Hatsopoulos. Propagating waves mediate information transfer in the motor cortex. *Nature Neuroscience*, 9:1549–1557, 2006.

[13] G. Bard Ermentrout and David Kleinfeld. Traveling electrical waves in cortex. *Neuron*, 29(1):33–44, 2001.

[14] Ali Bahramisharif, Marcel A. J. van Gerven, Erik J. Aarnoutse, Manuel R. Mercier, Theodore H. Schwartz, John J. Foxe, Nick F. Ramsey, and Ole Jensen. Propagating neocortical gamma bursts are coordinated by traveling alpha waves. *The Journal of Neuroscience*, 33(48):18849–18854, 2013.

[15] K. Takahashi, M. Saleh, R. D. Penn, and N. G. Hatsopoulos. The sleep slow oscillation as a traveling wave. *Front Hum Neurosci.*, 24(31):6862–6870, 2004.

[16] Evgueniy V. Lubenov and Athanassios G. Siapas. Hippocampal theta oscillations are traveling waves. *Nature*, 459(28):534–539, 2009.

[17] Honghui Zhang and Joshua Jacobs. Traveling theta waves in the human hippocampus. *The Journal of Neuroscience*, 35(36):12477–12487, 2013.

[18] Adam Keane and Pulin Gong. Propagating waves can explain irregular neural dynamics. *The Journal of Neuroscience*, 35(4):1591–1605, 2015.

[19] Lopes da Silva FH, Blanes W, Kalitzin SN, Parra J, Suffczynski P, and Velis DN. Dynamical diseases of brain systems: different routes to epileptic seizures. *IEEE Trans Biomed Eng*, 50(5):540–548, 2003.

[20] M. Ursino and G.E. La Cara. Traveling waves and eeg patterns during epileptic seizure: analysis with an integrate-and-fire neural network. *J Theor Biol.*, 242(1):171–87, 2006.

[21] M. A. Dahlem and E. P. Chronicle. A computational perspective on migraine aura. *Progress in Neurobiology*, 74:351–361, 2004.

[22] James Robert Brasic. Hallucinations. *Perceptual and motor skills*, 86:851–877, 1998.

[23] Peter Tass. Oscillatory cortical activity during visual hallucinations. *Journal of biological physics*, 23:21–66, 1997.

[24] Kristian P. Doyle, Roger P. Simon, and Mary P. Stenzel-Poore. Mechanisms of ischemic brain damage. *Neuropharmacology*, 55(3):310–318, 2008.

[25] Daniel Cremers. Traveling waves of excitation in neural field models: equivalence of rate descriptions and integrate-and-fire dynamics. *Neural Computation*, 14(7):1651–1667, 2002.

[26] S. Coombes. Waves, bumps, and patterns in neural field theories. *Biological Cybernetics*, 93:91–108, 2005.

[27] H. G. E. Meijer and S. Coombes. Traveling waves in models of neural tissue: from localized structures to periodic waves. *PJ Nonlinear Biomedical Physics*, 2(3), 2014.

[28] H. G. E. Meijer and S. Coombes. Traveling waves in a neural field model with refractoriness. *Journal of Mathematical Biology*, 68(5):1249–1268, 2014.

[29] Bard Ermentrout. The analysis of synaptically generated traveling waves. *Journal of Computational Neuroscience*, 5:1197–1221, 1998.

[30] Paul C. Bressloff. Traveling waves pulses in a one-dimensional network of excitable integrate-and-fire neurons. *Journal of Mathematical Biology*, 40:169–198, 2000.

[31] R. Osan and G. B. Ermentrout. The evolution of synaptically generated waves in one- and two-dimensional domains. *Physica D.*, 163:217–235, 2002.

[32] R. Osan, R. Curtu, J. Rubin, and G. B. Ermentrout. Multiple-spike waves in a one-dimensional integrate-and-fire neural network. *Journal of Mathematical Biology*, 48:243–274, 2004.

[33] R. Osan, R. Rubin, R. Curtu, and G. B. Ermentrout. Traveling waves in a one-dimensional integrate-and-fire neural network with finite support connectivity. *Neurocomputing*, 52-54:869–875, 2003.

[34] R. Osan and G. B. Ermentrout. Speed-up methods for simulations of traveling waves in integrate-and-fire neural networks. *Neurocomputing*, 52-54:863–868, 2003.

[35] Remus Osan, Jonathan Rubin, and Bard Ermentrout. Regular traveling waves in a one dimensional network of theta neurons. *SIAM J. Appl. Math*, 62:1197–1221, 2002.

[36] Remus Osan and Bard Ermentrout. Two dimensional synaptically generated traveling waves in a theta-neuron neural network. *Neurocomputing*, 38-40:789–795, 2001.

[37] David Golomb and Yael Amitai. Propagating neuronal discharges in neocortical slices: Computational and experimental study. *Journal of Neurophysiology*, 78:1199–1211, 1997.

[38] Laura R. Gonzalez-Ramirez, Omar J. Ahmed, Sydney S. Cash, C. Eugene Wayne, and Mark A. Kramer. A biologically constrained, mathematical model of cortical wave propagation preceding seizure termination. *PLoS Computationally Biology*, 11(2):e1004065, 2015.

[39] Paul C. Bressloff. *Waves in Neural Media: From single cells to Neural Fields*. Springer, 2013.

[40] Zachary P. Kilpatrick and G. Bard Ermentrout. Response of traveling waves to transient inputs in neural fields. *Physical Review E*, 85(021910), 2012.

[41] Paul C. Bressloff and Matthew A. Webber. Front propagation in stochastic neural fields. *Society for Industrial and Applied Mathematics*, 11(2):708–740, 2012.

[42] Zachary P. Kilpatrick and G. Bard Ermentrout. Coupling layers regularizes wave propagation in stochastic neural fields. *Physical Review E*, 85:021910, 2014.

[43] David J. Pinto and G. Bard Ermentrout. Spatially structured activity in synaptically coupled neuronal networks. *Society for Industrial and Applied Mathematics*, 62(1):206–225, 2001.

[44] J. A. Villacorta-Atienza and V. A. Makarov. Wave-processing of long-scale information by neuronal chains. *PLoS ONE*, 8(2):0057440, 2013.

[45] Paul C. Bressloff. Traveling fronts and wave propagation failure in an inhomogeneous neural network. *Physica D*, (155):83–100, 2001.

[46] N. V. Swindale. The development of topography in visual cortex: a review of models. *Network*, (7):161–247, 1996.

[47] Zachary P. Kilpatrick, Stefanos E. Folias, and Paul C. Bressloff. Traveling pulses and wave propagation failure in inhomogeneous neural media. *SIAM J. Applied Dynamical Systems*, (7):161–185, 2008.

[48] J. P. Keener. Propagation of waves in an excitable medium with discrete release sites. *SIAM J. Appl. Math.*, (61):317–334, 2000.

[49] Jie Zhang and Remus Osan. Analytically tractable studies of traveling waves of activity in integrate-and-fire neural networks. *Phys. Rev. E*, 93:052228, 2016.

[50] Wikipedia. Biological neuron models, 2016.

[51] Eugene M. Izhikevich. Which model to use for cortical spiking neurons? *IEEE TRANSACTIONS ON NEURAL NETWORKS*, 15(5):1063–1070, 2004.

[52] L. F. Abbott. Lapique's introduction of the integrate-and-fire model neuron(1907). *Brain Research Bulletin*, 50(5/6):303–304, 1999.

[53] Wulfram Gerstner and Werner M. Kistler. *Spiking Neuron Models. Single Neurons., Populations, Plasticity.* Cambridge University Press, 2002.

[54] S. Ostojic, N. Brunel, and V. Hakim. How connectivity, background activity, and synaptic properties shape the cross-correlation between spike trains. *Journal of Neuroscience*, 29(33):10234–10253, 2009.

[55] P. E. Latham, B. J. Richmond, P. G. Nelson, and S. Nirenberg. Intrinsic dynamics in neuronal networks. i. theory. *The American Physiological Society*, 83(2):808–27, 2000.

[56] G. B. Ermentrout and N. Kopell. Parabolic bursting in an excitable system coupled with a slow oscillation. *SIAM-J.-Appl.-Math*, 46(2):233–253, 1986.

[57] Scholarpedia. Ermentrout-kopell canonical model, 2016.

[58] A. L. Hodgkin and A. F. Huxley. A quantitative description of membrane current and its application to conduction and excitation in nerve. *The Journal of Physiology*, 117(4):500–544, 1952.

[59] A. L. Hodgkin and A. F. Huxley. Measurement of current-voltage relations in the membrane of the giant axon of loligo. *The Journal of Physiology*, 116(4):424–448, 1952.

[60] A. L. Hodgkin and A. F. Huxley. Currents carried by sodium and potassium ions through the membrane of the giant axon of loligo. *The Journal of Physiology*, 116(4):449–472, 1952.

[61] A. L. Hodgkin and A. F. Huxley. The components of membrane conductance in the giant axon of loligo. *The Journal of Physiology*, 116(4):473–496, 1952.

[62] R. Fitzhugh and E. Izhikevich. Fitzhugh-nagumo model. *Scholarpedia*, 1(9):1349, 2006.

[63] Koch Christof and Segev Idan. Methods in neuronal modeling: from ions to networks(2nd ed.). *MIT Press*, page 687, 2006.

[64] J. L. Hindmarsh and R. M. Rose. A model of neuronal bursting using three coupled first order differential equations. *Proc. R. Soc. Lond*, 221:87–102, 1984.

[65] H. R. Wilson and J. D. Cowan. A mathematical theory of the functional dynamics of cortical and thalamic nervous tissue. *Kybernetik*, 13(2):55–80, 1973.

[66] Jan Kujala, Julien Jung, Sandrine Bouvard, Francoise Lecaignard, Amelie Lothe, Romain Bouet, Carolina Ciumas, Philippe Ryvlin, and Karim Jerbi. Gamma oscillations in v1 are correlated with $gaba_a$ receptor density: A multi-modal meg and flumazenil-pet study. *Scientific Reports*, 46(5):16347, 1986.

[67] R. D. Chervin, P. A. Pierce, and B. W. Connors. Periodicity and directionality in the propagation of excitation in neural network model. *J. Neurophysiol.*, 60:1695–1713, 1988.

[68] D. Golomb and G. B. Ermentrout. Continuous and lurching traveling pulses in neuronal networks with delay and spatially decaying connectivity. *Proc. Natl. Acad. Sci. USA*, 106(5-6):13480–13485, 1999.

[69] Jonathan E. Rubin. A nonlocal eigenvalue problem for the stability of traveling wave in neuronal medium. *Discrete and Continuous Dynamical Systems*, 10(4)(4):925–940, 2004.